

Photochargeable Semiconductors: in “Dark Photocatalysis” and Beyond

Andrea Rogolino and Oleksandr Savateev*

Photochargeable semiconductors enable energy harvesting and storage in a single material. Charges separated upon absorption of photons can accumulate in highly energetic trap states if morphology, size, and chemical composition are appropriately chosen. For example, electrons can survive for several hours if hole scavengers are used to prevent their recombination with photogenerated holes, and their negative charge is balanced by positive counter-ions. The first database of charge-storing semiconductors is recently released, containing information from more than 50 publications within the past 40 years. Now, the database has been updated with more than 90 entries from the latest works on the topic. These materials have been largely utilized in the context of “dark photocatalysis”, that is, redox reactions enabled by photocharged semiconductors long after cessation of light irradiation. Nevertheless, a variety of further potential applications have not received enough visibility, including memory storage, steel anti-corrosion, sensors, and micromotors. In this review, the key figures of merit of photocharged semiconductors and the empirical relationships found between them is highlighted. After showing the latest advances in dark photocatalysis, it is discussed how other application fields may benefit from these materials. For each area, promising research directions based on the findings from the database are recommended.

electrical-powered devices that reduce our dependence on hydrocarbons. Nevertheless, this vision will only be effective if electricity is generated from renewable energy sources. Light irradiated from the Sun is a clean, worldwide accessible, and inexhaustible power that will inevitably drive many future technologies. Two key challenges need to be addressed for the utilization of light: energy harvesting and energy storage. We need materials capable of absorbing electromagnetic radiation and transferring their energy to do useful work, but this is not enough. Solar energy is inherently intermittent, which means research on strategies to store it—for example in batteries or solar fuels like hydrogen—is equally fundamental. Semiconductors are ubiquitous in light-harvesting technologies, epitomized by silicon-based photovoltaic cells.^[1] The underlying principle of all light-matter interaction is the transition from the ground state to an excited one. In a common scenario for inorganic semiconductors, upon ultraviolet (UV) and visible light irradiation, electrons are promoted to the empty conduction band (CB) while

holes are left in the valence band (VB).^[2] To contrast this unstable electronic configuration, accumulated carriers are then usually transferred to chemical species for catalytic purposes or recombined with either emission of light or energy transfer, that is relevant to analytical or imaging methods.^[3] Nevertheless, under certain circumstances accumulated electrons can survive in the material, provided that holes are scavenged by an electron-donating species and replaced by positive counter-ions to ensure charge balance. Holes accumulation, although less common, can equivalently occur in the presence of electron scavengers and negative counter-ions. This phenomenon is known as photocharging or photodoping.^[4] Essentially, these semiconductors are charged like batteries with light and slowly discharged in the dark. For photocharging to occur, a number of conditions must be satisfied: i) charges must accumulate into highly energetic trap states, that kinetically suppress relaxation or charge transfer; ii) to prevent electron-hole recombination, unwanted carriers must be removed by (possibly sacrificial) scavengers: electrons and holes accumulation require hole and electron scavengers, respectively; iii) high amounts of stored charge must be balanced by counter-ions, the most common being H^+ , Na^+ , K^+ in the case of electron accumulation (**Figure 1**).^[5] Photocharging was first

1. Introduction

Social, political, and environmental changes are urging countries around the world to make a transition from a fossil to a renewable-based industry. Actions are being taken to spread

A. Rogolino
Cavendish Laboratory
University of Cambridge
JJ Thomson Ave, Cambridge CB3 0HE, UK

O. Savateev
Department of Colloid Chemistry
Max Planck Institute of Colloids and Interfaces
Am Mühlenberg 1, 14476 Potsdam, Germany
E-mail: oleksandr.savateiev@mpikg.mpg.de

The ORCID identification number(s) for the author(s) of this article can be found under <https://doi.org/10.1002/adfm.202305028>

© 2023 The Authors. Advanced Functional Materials published by Wiley-VCH GmbH. This is an open access article under the terms of the Creative Commons Attribution License, which permits use, distribution and reproduction in any medium, provided the original work is properly cited.

DOI: 10.1002/adfm.202305028

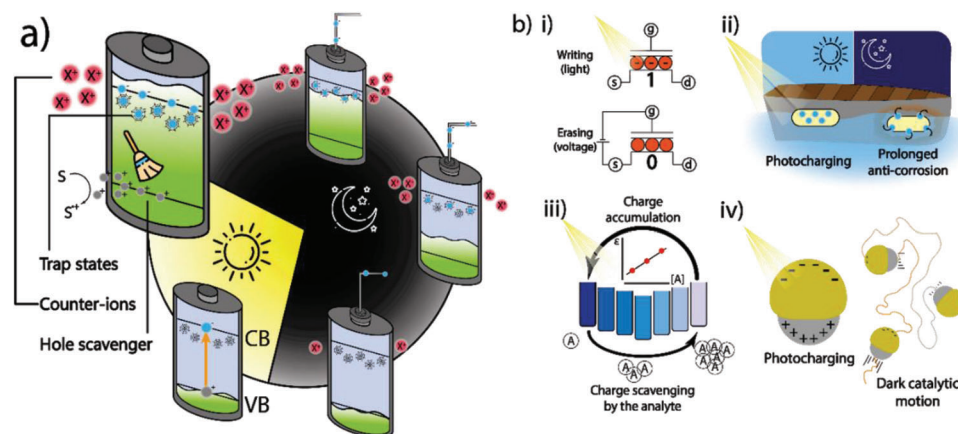


Figure 1. a) Schematic working principle of photocharged semiconductors around a charge–discharge cycle. b) Summary of possible applications of photocharged semiconductors beyond dark photocatalysis: i) devices for memory storage; ii) photoanodes for anti-corrosion in naval engineering; iii) sensors and analytical methods; iv) light-fueled micromotors, or microswimmers.

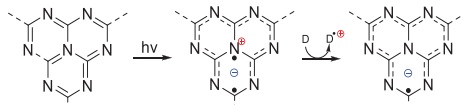
demonstrated in the 1980s on colloidal TiO_2 suspensions.^[6] In this example, electrons were trapped on Ti atoms that undergo Ti(IV)-to-Ti(III) reduction, propan-2-ol was added as a hole scavenger and protons from the acidic environment served as counter-ions. Photocharging is also commonly manifested with a change in optical properties, sometimes visible to the naked eye. For example, a suspension of TiO_2 nanoparticles turns from colorless to blue upon UV irradiation and retains this appearance for several minutes.^[7,8] The phenomenon, known as “photochromism”, has stimulated interest in technologies like “smart” windows.^[9] A general mechanistic understanding of semiconductor photocharging is still far from being achieved, but likely scenarios for a few categories of materials can be identified (Table 1). TiO_2 and ZnO nanoparticles are expected to undergo $1e^-$ reduction on metal centers, lowering the oxidation state of the metal.^[10] The same is proposed for metal–organic frameworks (MOFs).^[11] In polymeric carbon nitrides (PCN), electrons and holes are first separated by localization on C or N atoms upon irradiation. A hole scavenger depletes the material of positive charges, leaving C- or N-centered radicals.^[12] Materials including WO_3 , MoO_3 , and SnO_2 can trap electrons in the presence of alkali metal cations (M^+) by forming relatively stable bronzes like $M_x\text{WO}_3$.^[13] Charge accumulation in other materials such as quantum dots (QDs) is usually not well defined. Generally, it is ascribed to charge trapping

in unspecified defect states, although inorganic nanoparticles like ZnS , ZnSe , or CdSe could reasonably behave as TiO_2 and ZnO .^[14]

Savateev recently created the first database of photocharged materials and summarized the key findings in a review.^[5] The full list of data and plots—available at pccmat.mpikg.mpg.de—is a catalog of light-sensitive, charge-accumulating materials collected from the literature published in the past 40 years. The materials have been systematically described according to their charge-storing capacity, rate of photocharging, and rate of discharging in the dark. Experimental conditions including irradiation source, counter-ions, and hole/electron scavengers were also included. The database has been now updated with the latest relevant publications released in the past two years, summing up to 94 new entries from 16 references. The goal of the database is to stimulate data-driven research toward rational designs of materials for diverse applications.

The new set of data examined does not significantly alter the conclusions drawn in the previous work. Most of the new entries fit in the trends previously identified, which are briefly summarized in Section 2 of this manuscript. With such marginal expansion of the database, no new information in terms of the fundamental mechanisms of photocharging can be derived. Instead, a careful revision of the recent literature led us to discover a variety of applications majorly not covered in the first version of

Table 1. Proposed photocharging mechanism for some categories of materials.

Material	Proposed mechanism	Examples of related chemical reaction ^{a)}
TiO_2 , ZnO nanoparticles. Possibly MOFs and QDs.	$1e^-$ reduction of metal centers	$\text{Ti(IV)} + e^- + h^+ + \text{D} \rightarrow \text{Ti(III)} + \text{D}^+$
Polymeric carbon nitrides	Charge separation and hole scavenging	
WO_3 , MoO_3 , SnO_2	Formation of bronzes	$\text{WO}_3 + M^+ + xe^- + h^+ + \text{D} \rightarrow M_x\text{WO}_3 + \text{D}^+$

^{a)} D indicates an electron donor or hole scavenger.

the database. Previous entries majorly referred to the new concept of “solar batteries”,^[15,16] or the more deeply investigated “dark photocatalysis”. This relatively new research area involves materials with time-delayed photocatalytic activity. Unlike conventional photocatalysis, which requires an uninterrupted supply of photons, in dark photocatalysis photocharged semiconductor serves as a chemical reductant and therefore does not require continuous irradiation.^[17] Ionic polymeric carbon nitrides have received special attention as inexpensive organic polymers with time-delayed photocatalytic activity in the hydrogen evolution reaction (HER) and organic transformations.^[17–19] Nevertheless, the variety of sources in the database indicates that several potential uses of photocharged semiconductors may have been simply neglected. In particular, we identified four relevant areas other than dark photocatalysis: 1) devices for memory storage; 2) photoanodes for anti-corrosion in naval engineering; 3) sensors and analytical methods; 4) light-fueled micromotors, or microswimmers (Figure 1b). Information can be written in transistor-based non-volatile memory devices through the irradiation of charge-storing particles that create a gate voltage. It is then erased by voltage pulses (Figure 1b,i). Sacrificial and non-sacrificial anodes for the photocathodic protection of steel can accumulate electrons during the day and slowly release them in the dark to prevent metal oxidation (Figure 1b,ii). The electron and hole-scavenging ability of suitable analytes can induce changes in the optical properties of nanoparticle suspensions that exhibit photochromism. The proportionality between the concentration of the scavenger and the color shift can translate into calibration curves for quantitative analysis (Figure 1b,iii). Janus particles that photocatalyze propulsion-generating reactions can exhibit prolonged motion after photocharging (Figure 1b,iv).

Here, we first summarize the key findings of our systematic data analysis. We highlight plausible trends observed between characteristic parameters of photochargeable materials, such as the charge-storing capacity as a function of the size of semiconductor nanoparticles. Comments on how the latest entries fit with previous data are made where relevant. Next, we describe the latest advances in dark photocatalysis, with an emphasis on new materials including MOFs, hole-storing BiVO₄, and covalently-functionalized PCN. Further application fields are discussed in the following sections. For each, a brief background on the technology, the relevance of photocharged materials, and examples from the literature are provided. In our conclusion, we summarize the key features that the ideal photochargeable semiconductor should have for each of the applications proposed. Based on the trends observed from the database and examined in the first section, we recommend the materials that might give the best performance in each field.

2. Observed Trends from Systematic Data Analysis

Data collected from over 70 references published in the last 40 years, for a total of 398 entries, were systematically analyzed to identify key parameters that govern the performance of semiconductor photocharging, as well as their possible mutual relationships. The main parameters considered were: (i) the average maximum number of electrons stored per particle ($\langle n_{\max} \rangle$); (ii) the maximum molar amount of electrons stored

per mass of material, or—by analogy with batteries—the capacity (δ_{\max} , mol g⁻¹); (iii) the specific initial rate of photocharging (R_{PC} , mol g⁻¹ s⁻¹); (iv) the specific initial rate of discharging in the dark (R_{DC} , mol g⁻¹ s⁻¹). Different methods are available to determine these figures of merit, but most commonly, accumulated electrons in transparent suspensions of nanoparticles are quantified by spectrophotometric titration. Redox indicators such as Fe³⁺ salts or methyl viologen are used as titrants. Changes in the color of the suspension due to photochromism and to the indicator itself can be monitored by means of UV–vis spectrophotometry. Knowing the stoichiometry of the electron quenching by the redox indicator (e.g., one mole of electrons is quenched by one mole of Fe³⁺), the capacity of the material (δ_{\max}) can be calculated. If particles are spherical, relatively monodisperse, and the density of the material (or, equivalently, the crystalline structure and the cell parameter) is known, the average number of electrons accumulated per particle ($\langle n_{\max} \rangle$) can also be derived.^[20] In the case of non-transparent suspensions, where spectrophotometry is limited by scattering, other approaches including electron paramagnetic resonance (EPR) spectroscopy^[21] or electrochemical methods can be chosen.^[22] The initial rates of photocharging and discharging are theoretically defined as the slope of the δ – t curve at the time when irradiation is turned on and off, respectively. Due to practical constraints, these are often approximated as the ratio of accumulated or discharged electrons in the shortest time accessible to experimental techniques (e.g., spectrophotometry), expressed as $\Delta\delta/\Delta t$. While the determination of R_{PC} necessarily requires quantifying the accumulated charges at different irradiation times, R_{DC} is more easily quantified by indirect methods. For example, the initial rate of discharge can be calculated from the initial rate of hydrogen evolution in the dark, assuming that one mole of H₂ is generated every two moles of discharged electrons.^[17] For a thorough discussion of methods and full results, the reader is referred to the review by Savateev.^[5] The database, recently expanded with 94 new entries, cover a wide range of materials, including mostly TiO₂, ZnO nanoparticles, and polymeric carbon nitrides. Because of such high diversity in chemical features and experimental conditions, data points hardly suggested any global pattern that could define universal characteristics. Nevertheless, we identified some trends, though in some cases limited to specific categories of materials. Key relationships are summarized below and illustrated in **Figure 2**:

- $\langle n_{\max} \rangle$ scales linearly with the volume of nanoparticles (V_{p}).
- R_{PC} increases with δ_{\max} for TiO₂ particles up to 20 nm in diameter.
- R_{DC} decreases with the volume of nanoparticles (V_{p}).
- R_{DC} increases with higher concentrations of electron acceptor (C_{A}).

It is important to remind that these trends are the result of empirical observation, simply deriving from the distribution of data points from the pool of references examined (Figures S1–S4, Supporting Information). Therefore, Figure 2 only provides a visual summary of the most meaningful relationships identified from systematic data analysis. Proposing a rationale for the observed trends—if of any significance—goes beyond the scope of this work, but some speculations can be made. Behavior a) was

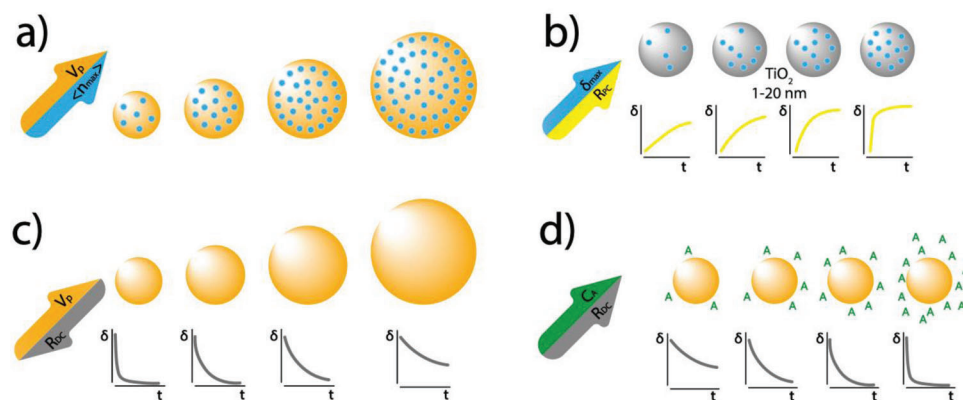


Figure 2. Main trends observed between key parameters of photocharged semiconductor nanoparticles. a) $\langle n_{\max} \rangle$ is linearly proportional to V_p . b) R_{PC} is proportional to δ_{\max} for 5–20 nm TiO_2 nanoparticles. c) R_{DC} decreases for bigger nanoparticles. d) R_{DC} is proportional to C_A .

observed over different categories of material, regardless of experimental conditions. The outcome is easily expected on account of simple geometric reasons: higher volumes host more trapping sites for photoexcited electrons. It is important to stress that $\langle n_{\max} \rangle$ can provide significantly different insights compared to the specific capacity δ_{\max} expressed in terms of the quantity of electrons per mass of materials. The latter is intrinsically dependent on the density of the material, while the former provides information at the atomic level. Indeed, the number of accumulated electrons can be traced back to the number of reduced sites on the materials, usually corresponding to metal centers (including Ti^{IV} and Zn^{II}) undergoing $1e^-$ reduction. It is, therefore, a useful metric to quantify the fraction of electron-storing atoms in a nanoparticle, or alternatively the density of charge-trapping defects. Trend b) is an interesting finding. The relationship seems to suggest that if TiO_2 nanoparticles can host a higher number of electrons, these will experience a stronger driving force to be accumulated in the semiconductor. In other words, the time needed to saturate TiO_2 nanoparticles with electrons is approximately constant, and equal to the reversed slope of the R_{PC} - δ_{\max} dependence (Figure S1, Supporting Information). However, it is common for trends observed in big data to arise from indirect relationships. In particular, we speculate that an increase in the rate of photocharging should be primarily ascribed to specific surface area (S_{SA}). An increase in surface area is supposed to expose more anchoring sites to counter ions, allowing to balance a greater build-up of photogenerated charges. A plot of R_{PC} versus S_{SA} revealed a positive relationship for Ti-based particles sized 1–20 nm (Figure S2, Supporting Information). S_{SA} might be a better predictor of the rate of photocharging, so materials with high porosity should be preferred for applications requiring fast electron accumulation, like memory devices discussed in Section 4. However, environmental conditions including counter-ions, pH, and light intensity all contribute to R_{PC} , thus tracing it back to a single parameter might be naive indeed. Trends c) and d) are probably the most relevant to the design of photochargeable devices with delayed release of stored electrons. Indeed, most applications would benefit from a slow discharge process, so that accumulated charges can be harnessed for longer times in the dark. For example, photocharged materials with low discharging rates prevent metal corrosion for longer times in cathodic protection

(Section 5) and propel microswimmers across longer distances (Section 7). The discharging process is highly influenced by the volume of the nanoparticles. Non-porous materials based on titanium and zinc oxides between 20 and 30 nm in diameter released photogenerated electrons up to seven orders of magnitude more slowly than 1 nm particles (Figure S3, Supporting Information). As discussed in point b), the transport of counter-ions is supposed to be the rate-determining process of electron accumulation/release for bigger volumes or surface areas. For electrons to be discharged, counter-ions should follow them closely to balance charges on the semiconductor. If electrons left the semiconductor with no simultaneous diffusion of counter-ions, this would result in a build-up of positive charge on the material, eventually not stable. For example, when electrons initially counter-balanced by H^+ ions on a semiconductor are transferred to an acceptor (A) in solution, the reduced species (A^-) will rapidly diffuse away from the surface of the material. For higher thermodynamic stability, the species A^- should be paired with a H^+ ion coming from the material. For that reason, higher mobility of counter ions is important regardless of the discharging mechanism. While electrons are generated in the bulk, counter ions can either only adsorb on the surface (large organic cations) or intercalate into the bulk (H^+ and small metal cations). The surface-to-volume ratio decreases for larger spherical nanoparticles, resulting in impaired simultaneous transfer of electrons and counter-ions. This trend was confirmed by data entries from recent works on TiO_2 photocharging (Figure S3, Supporting Information). Interestingly, >200 nm large porous particles like MOFs exhibited discharging rates comparable to ten times smaller non-porous materials, confirming that semiconductors with a microporous structure allow faster diffusion of counter-ions in and out of the material.^[11] A thorough understanding of surface pathways is only accessible with advanced electrochemical methods. Near ambient pressure operando X-ray photoemission spectroscopy (XPS) is a valid technique for this purpose.^[23] Finally, observation d) was valid for a variety of TiO_2 and ZnO nanoparticles and is easily explained by a higher driving force for electron extraction (Figure S4, Supporting Information). When aiming for the prolonged release of electrons, electron acceptors should be fed continuously and kept at low concentrations, possibly with flow methods.

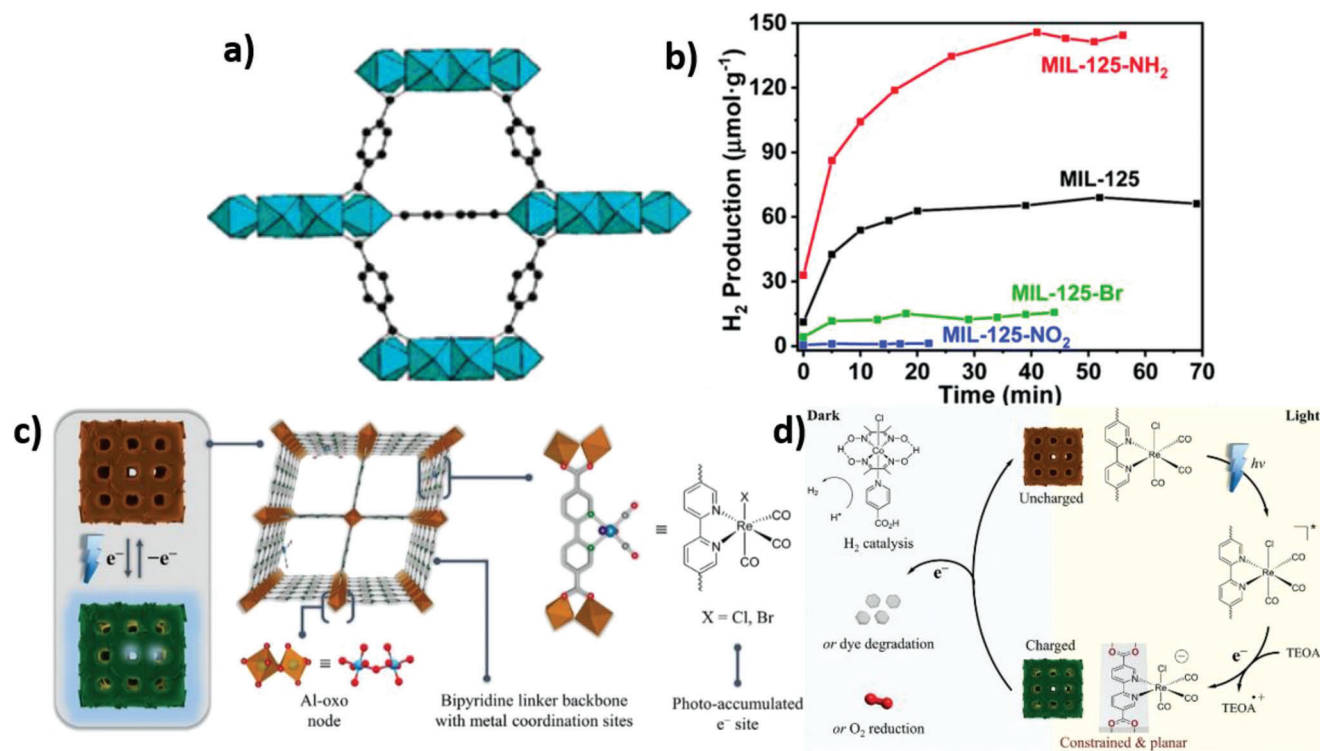


Figure 3. a) Illustration of MIL-125, with TiO₅(OH) clusters represented as blue prisms and DBC as balls and sticks. b) Dark photocatalytic hydrogen generation of MIL-125 comprising different functional groups after 1 h irradiation in the presence of TEOA. Reproduced with permission.^[25] Copyright 2022. Royal Society of Chemistry. c) Scheme of the photocharging of a Re-based MOF-253, including DCbipy linkers. d) Scheme of the proposed mechanism of photocharging and dark catalysis upon discharging of the Re-based MOF-253 illustrated in (c). Reproduced with permission.^[26] Copyright 2023. John Wiley & Sons.

3. Dark Photocatalysis

So-called “dark photocatalysis”, or “around-the-clock” photocatalysis, is certainly the most prominent application of photocharged semiconductors. The term refers to the time-decoupled utilization of light to enable chemical reactions. Photons are stored in the form of photogenerated carriers that are later transferred to the desired substrate. The concept is especially relevant to redox reactions, with the hydrogen evolution reaction (HER) being the most represented.^[17,24–26] Numerous reviews and discussions have been dedicated to the topic,^[27,28] so here we only summarize photochargeable materials explored in the past recent years.

More than 40% of photochargeable semiconductors are based on titanium, most commonly present by TiO₂ anatase nanoparticles.^[5,7,20] However, Rose et al. proposed an innovative synthesis procedure and application of this ubiquitous material in the form of mesoporous aerogels. Materials were prepared via a sol–gel method and a different porosity was achieved depending on the calcination temperature. Light-driven electron accumulation was immediately evident from the color change of a colloidal suspension from colorless to blue, a typical photochromic effect indicating Ti⁴⁺-to-Ti³⁺ conversion.^[7,8] Notably, this was only observed in a methanol solution, where the hole-scavenging solvent suppresses charge recombination. Dark photocatalytic hydrogen generation was achieved, with a sharp peak in hydrogen production registered upon the addition of H₂PtCl₆ catalyst 1 h after prolonged irradiation. Most interestingly, increased porosity was

inversely related to the electron storage capacity of the aerogels, with the highest δ (220 µmol of electrons g⁻¹) obtained for the as-synthesized aerogel that was not subjected to thermal treatment. Higher calcination temperatures resulted in lower specific surface area and lower charge-storing capacity. This was attributed to the reduced amount of surface defects on the thermally annealed material, where photogenerated electrons are supposed to be trapped. However, the opposite trend was observed for the photocatalytic HER activity. This finding was tentatively explained by the exposure of catalytically active facets upon thermal treatment.

While the vast majority of works on semiconductor photocharging are linked to anatase and zinc oxide nanoparticles, MOFs have recently attracted interest for their high porosity that enables superior electron-storage capacity. Photocharging was previously reported for Co-^[29] and Ti-based^[30,31] MOFs. However, the ability to store charges was only verified by looking at enhanced conductivity or photochromism. The first application of Ti-MOFs in dark photocatalysis was reported by Pan et al.^[25] Photochromic MIL-125 (Figure 3a),^[30] including TiO₅(OH) centers linked by 1,4-dibenzenecarboxylate (DBC), successfully catalyzed hydrogen evolution when mixed with a Pt catalyst in the dark after 1 h of visible light irradiation in the presence of triethanolamine (TEOA) as the electron donor. More interestingly, the authors demonstrated that the number of stored electrons and the resulting activity in dark photocatalysis was highly dependent on the functional groups introduced in the

organic linkers. In particular, when an H atom in the aromatic ring of the DBC carboxylate linker was replaced with Br, hydrogen evolution dramatically decreased, and it was totally suppressed with NO₂ as the substituent. Conversely, when NH₂ was chosen as the functional group, the total amount of hydrogen evolved more than doubled (Figure 3b). The difference in observed activity is likely attributed to the electron-donating or electron-withdrawing nature of the organic linker. Thorough characterization involving UV–vis, photoluminescence (PL), and electron paramagnetic spectroscopy (EPR), confirmed that MIL-125-NH₂ increases the yield of Ti^{IV}-to-Ti^{III} photoreduction as well as the lifetime of stored electrons. Moreover, time-dependent density functional theory (TD-DFT) studies revealed that the introduction of electron-donating/-withdrawing groups shifts the energy of the lowest unoccupied molecular orbital (LUMO) of MIL-125 downward/upward, respectively. Electronically-excited MIL-125 functionalized with electron-donating groups is more reductive, which results in a higher yield of hydrogen. Overall, the work demonstrates that light-induced electron accumulation and storage in photoactive materials, such as MOFs, prepared by bottom-up techniques, may be tuned by the chemical engineering of their building blocks. Although evidence of photochromism in MOFs was mostly reported for Ti-based frameworks, very recently Stanley et al. proposed to use Re centers for solar-driven electron storage.^[26] MOF-253, including 5,5'-dicarboxy-2,2'-bipyridine (DCbipy) linkers, was used as a platform to introduce Re(CO)₃X (X = Cl, Br) centers coordinated by bipyridine nitrogen atoms, yielding ReCl-253 and ReBr-253. The obtained powders changed color from brown to dark green upon irradiation (Figure 3c). Although Re(CO)₃X centers are well-known photocatalysts for CO₂-to-CO conversion,^[32] no CO₂ reduction occurred in the presence of ReX-253 and visible light. This outcome was attributed to the generation of a trapped radical anion, where the removal of X⁻—an essential step in the mechanism of CO₂ reduction—is prevented. EPR spectroscopy confirmed the presence of a stable radical anion species. Moreover, DFT calculations showed that the anionic Re centers generated upon photocharging in MOF-253 are more stabilized than the corresponding anions in the free complex. The authors attributed this extra stabilization to the constrained geometry of bipyridine ligands induced by the reticulate structure. The material could be charged up to a capacity of 15 C g⁻¹ (0.16 mmol e⁻ g⁻¹). The accumulated electrons were stored for more than one month and were successfully utilized for hydrogen evolution and dye degradation in the dark over ten cycles with only 10% overall losses (Figure 3d).

Electrons are the preferred carriers to be accumulated because of the prevalence of n-type systems. Bismuth-based nanoparticles are an emerging class of semiconducting materials relevant to hole storage, instead. Bismuth or bismuth-metal oxides, exemplified by the state-of-the-art BiVO₄ largely applied in photoanodes for oxygen evolution,^[33] are known photocatalysts with bandgaps generally lying in the region of visible light.^[34] Charge storage was demonstrated for bismuth oxides coupled to silver nanoparticles. In particular, dark photocatalytic activity for BiO_{2-x} was greatly enhanced when Ag particles were adsorbed on the surface of the oxide.^[35] No memory effect was detected for BiO_{2-x} alone, which points toward a transfer of photogenerated electrons from the bismuth oxide to peripheral Ag particles. Thus,

BiO_{2-x} behaves as an efficient hole sink. This delocalization of charge is believed to extend the excited carriers' lifetime. Ag-BiO_x systems are especially beneficial for hole storage. Wang and co-workers reported that Ag deposition on BiO_{2-x}/Bi₂O_{2.75} composite increased the concentration of stored holes by 11.45 times, while electron storage only increased by 3.46 compared with the Ag-free semiconductor.^[36] It is proposed that holes are efficiently formed from oxygen vacancies on BiO_{2-x}/Bi₂O_{2.75} and electrons are transferred to the silver nanoparticles.

Polymeric carbon nitrides (PCN) represent the most promising alternative to Ti and Zn-based semiconductors for light-driven electron storage. Several examples of PCN photocharging have been reported,^[17,22,28,37–39] with the most valuable results found for ionic carbon nitrides, that is PCN containing Na⁺, K⁺, or Li⁺. The presence of cations in the polymeric structure is proposed to be at the foundation of photocharging. This observation applies both to materials prepared by modification of melon-like carbon nitrides with potassium thiocyanate (usually called “cyanamide-functionalized” carbon nitrides)^[17] or crystalline poly (heptazine imides) (PHIs) synthesized by ionothermal treatment, that is the co-polymerization of urea, melamine or dicyandiamide with Na, K or Li salts.^[19,40,41] Ionic carbon nitrides can store charges even in the absence of electron donors, as was demonstrated for PHIs gelled in ionic liquids.^[42] It was proposed that light irradiation induces the desorption of cations from ionic carbon nitrides, which in turn reduces the contribution of nitrogen to the conduction band. The new electronic configuration achieved thanks to the high mobility of cations results in a lower band gap, and thus to photochromism. Moreover, computational work showed that, unlike melon-like PCN, PHIs in both their charged and uncharged states possess an indirect band gap, which reduces the probability of charge recombination.^[42] This is consistent with a suppression of photoluminescence observed in PHIs compared to non-ionic PCN.^[40] Recently, Kröger et al. proposed a covalently functionalized PHI (Mel-PHI) where dangling cyanamide (NCN⁻) groups are converted to an isolated melamine ring by reaction with dicyandiamide (DCDA), essentially extending the aromatic graphitic structure (Figure 4a).^[38] The introduction of a terminal melamine unit was found to improve the interaction with the hole scavenger TEOA, with improved photocatalytic activity and hole quenching. This was also reflected by a prolonged electron storage efficiency, with 61% of accumulated charges retained after 2 h in the dark. Interestingly, dark photocatalysis for hydrogen evolution proceeded with much higher yields using TEOA rather than MeOH (Figure 4b). This evidence further confirmed the relevance of an improved TEOA-Mel-PHI interaction, due to the conversion of the ionic NCN⁻ moieties to hydrophobic melamine units. Imparted hydrophobicity also resulted in a more uniform deposition of PHI on electrodes for photoelectrochemical studies, as previously reported for other hydrophobic functionalizations.^[43] Improved adhesion led to charge stability over longer times, which is relevant for the design of solar batteries or day–night photoelectrocatalytic cells. The outcome of this work can be extended to all photochargeable semiconductors. A strong material-electron donor interaction suppresses electron-hole recombination and, in turn, is expected to increase δ_{\max} and R_{PC} values.

Dark photocatalysis has almost exclusively pertained to heterogeneous catalysis, given the predominance of nanoparticles,

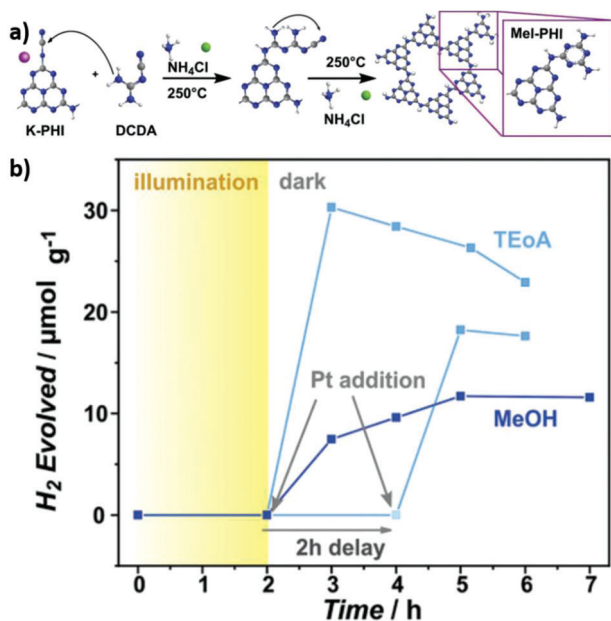


Figure 4. a) Scheme of Mel-PHI synthesis by functional group interconversion of cyanamide dangling moieties. b) Evolution of hydrogen in the dark upon the addition of Pt nanoparticles after irradiation under visible light for 2 h. Reproduced with permission.^[38] Copyright 2020. John Wiley & Sons.

bulk, and polymeric semiconductors among photochargeable materials. Recently, the very first molecular photochargeable species based on a photosensitizer-polyoxometalate (PS-POM) dyad was reported.^[44] The work combined the light-absorbing properties of state-of-the-art tris(bipyridine)ruthenium(II) complexes with the well-known properties of polyoxotungstate as charge-separating centers. In particular, the authors covalently attached a ruthenium-based dye to a Dawson POM through phosphonate bonds. After functionalization, the emission of the photosensitizer was quenched by 97%, indicating charge transfer to the POM. Importantly, a much lower quenching was observed when the Ru complex and the polytungstate were simply mixed in solution, suggesting that covalent bonding was crucial for efficient charge separation. By means of ultrafast absorption spectroscopy, it was concluded that excitation at 470 nm first induces the reduction of the photosensitizer, which in turn transfer electrons to the W centers on the Dawson POM, corresponding to a W^{VI}-to-W^V reduction. A combination of UV-vis spectroscopy and spectroelectrochemistry revealed that the PS-POM composite can accumulate up to 1.96 electrons per molecule, reaching saturation after only 6 min of irradiation in an anhydrous, de-aerated DMF solution containing ascorbic acid as the electron donor. Stored electrons were also successfully utilized for hydrogen evolution. Upon addition of H₂SO₄ as a proton source in the dark after a few minutes of irradiation, the PS-POM was totally discharged in 2 s generating H₂. If stored in an oxygen-free and water-free environment, the PS-POM composite was shown to retain a significant fraction of the accumulated electrons for at least 2.5 h. Although far from being competitively applied as a dark photocatalyst, the PS-POM was the first demonstration of a homogenous charge-storing system.

Finally, a proof of concept on polymeric organic materials with potential applications in dark photocatalysis was recently provided. Although PCN is by far the most studied and promising photoactive polymeric C-based material, research on organic polymers is pushing metal-free semiconductors forward.^[45] Typical organic nanoparticles with photocatalytic properties are based on donor/acceptor heterojunctions, often including fluorenyl and thiophene moieties.^[46] Kosco and co-workers adopted time-correlated spectroscopy tools to find relatively long-lived (up to seconds timescales) electrons upon irradiation of a nano-assembled blend of electron donor polymer PM6 and electron acceptor molecules Y6 or fullerene-derived PCBM.^[47] The two components of the investigated organic nanoparticles have suitable band positions to favor electron-hole separation, with the lowest unoccupied molecular orbital (LUMO) of the acceptor molecules still higher than the H⁺/H₂ standard reduction potential, which is relevant to photocatalytic hydrogen evolution. Advanced photophysical characterization included steady-state PL and transient absorption spectroscopy (TAS) to shine light on the electron transfer between donor and acceptor. Donor PM6 alone exhibited strong PL, which was quenched by > 95% when it was blended with acceptor Y6 or PCBM. Moreover, the signal from photogenerated excitons on PM6 decayed in the timeframe of ps because of the electron transfer to the acceptor molecule. This piece of evidence supported fast and efficient charge separation. Next, the authors determined the lifetime of photogenerated carriers by examining the spectral feature of PM6⁺, that is of the holes accumulated on the donor. Photoinduced absorption spectroscopy (PIAS) measurements showed that the spectral features of photogenerated holes survived for up to 4 s after illumination. The intensity of the signal was higher for PM6/PCBM than for PM6/Y6, which is consistent with the higher external quantum efficiency (EQE) in photocatalytic hydrogen evolution observed for the former. Most strikingly, such long-lived carriers were generated without any co-catalyst or hole/electron scavenger, while this is often required for inorganic semiconductors or polymeric carbon nitrides.^[48] Indeed, the intensity of the PIAS photogenerated holes signal increased in the presence of Pt nanoparticles as co-catalyst—as a consequence of electron transfer from Y6/PCBM to Pt, preventing charge recombination—and drastically decreased in the presence of ascorbic acid as a hole scavenger. Although the very brief characteristic charge storage time (4 s) cannot pertain to the field of dark photocatalysis, the work highlights the potential of highly tuneable donor/acceptor organic polymers for improved charge separation. In the future, it will be possibly pushed to the minutes timescale.

4. Non-Volatile Memory Devices

Charging and discharging processes constitute the working principle of transistor-based memory (TBM) devices.^[49–51] Information is stored in binary form depending on the state of each device (charged or uncharged). The fundamental components of all transistors are: i) two conductive terminals, a source and a drain, between which current is generated by applying a bias (V_{DS}), and ii) a conductive gate, which accumulates charges depending on its applied voltage (V_G). Non-volatility, which is the long-term stability of the 1 or 0 state, is crucial for TBM. To address this goal, the most common devices contain a “floating gate” between the

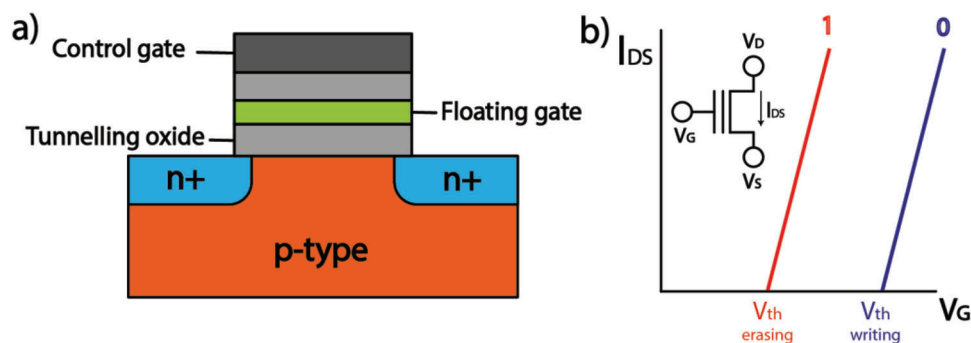


Figure 5. a) Scheme of a generic floating-gate TBM device for non-volatile energy storage. b) Equivalent circuit of a generic transistor and I_{DS} versus V_G curve for a device in its “1” or “0” state.

active (or control) gate and the source-drain layer (Figure 5a). In this configuration, the charge or discharge of the floating gate can only be induced by a high enough V_G . Consequently, electrons or holes in the floating gate cannot easily escape, and information is permanently stored until an “erasing” V_G is applied again. Information is read by measuring the current between the source and the drain (I_{DS}) at a given V_{DS} and V_G . Equivalently, an I_{DS} versus V_G plot can be recorded, as this is shifted depending on the state of the transistor (Figure 5b). For each state, the V_G at which the current starts to flow is defined as the threshold voltage (V_{th}). The difference between the threshold voltages (ΔV_{th}) of the two states determines the memory window. The optimal TBM device should have: i) low volatility, ii) fast writing time, iii) large memory window, and iv) high endurance, that is stability over multiple charge/discharge cycles.^[51]

Using light for information writing/erasing is an interesting venue to reduce power consumption and expand the memory window.^[52] This strategy has been especially explored in organic field-effect transistors.^[53] It is also expected that ultrafast irradiation results in lower long-term damage than gate voltage pulsing, ultimately leading to improved device lifetime.^[51] Photonics TBM devices have also been tested for multilevel data storage with promising results.^[54] Most of photochargeable semiconductors that have been investigated in the last decades are in the form of nanoparticles.^[5] Incidentally, this represents a great opportunity for TBM devices, which are nowadays exposed to great challenges set by their progressive miniaturization. The reduced sizes of transistors come with two main issues: i) difficult fabrication methods, and ii) limited charge storage capacity in floating gates. Nanoparticles provide a solution to both points. Suitable deposition methods such as spin-coating allow depositing nanometer-wide few layers to monolayers of nanoparticles on conducting substrates. Moreover, electrons and holes in photocharged nanoparticles are stored in highly dense trap states—compared to bulk semiconductor floating gates—which also prevents excessive charge leakage.^[50,55] The field of optoelectronic devices for non-volatile memory storage has been dominated so far by semiconducting quantum dots (QDs), by virtue of their ease of processability, fast photoresponse, and tuneability.^[51] One of the first applications of QDs in photore sponsive memory devices was proposed in 2008 by Chen et al.^[56] The device was fabricated in the usual TBM fashion: an n+ silicon gate surmounted by a SiO_2 insulator was covered with the

QD-based active layer and two finger-like Au/Ti electrodes on opposite sides functioned as source and drain. The active layer was a blend of poly(3-hexylthiophene) (P3HT) and trioctylphosphine oxide (TOPO)-capped CdSe QDs. This composite had already been applied in photovoltaics, where photogenerated excitons in CdSe were shown to dissociate by hole transfer to P3HT.^[57] The authors measured how I_{DS} evolved at a constant V_{DS} and V_G when the device was irradiated under a tungsten halogen lamp. The current steadily increased during illumination and decayed slightly when the light was turned off, reaching a metastable state. Then, when a fast (100 ms) negative V_G pulse was applied, the current dropped back to the starting level (Figure 6a). Overall, the work demonstrates the applicability of QDs as light-driven charge-storing materials in memory devices with optical writing and electrical erasing. Advances in similar QD-based devices gave rise to several variations, especially thanks to the adjustable optical properties of these materials. For example, CdSe/ZnS core-shell particles were synthesized to fabricate UV-responsive devices.^[58] Core-shell architecture was also recently investigated for InP/ZnS particles that exhibited optically-induced and electrically-induced electron and hole storage, respectively (Figure 6b).^[59] On average, InP/ZnS QDs could sustain 1.28 electrons and 1.64 holes per particle when irradiated with a 405 nm laser for 150 s. Information was stored with no decay for almost 3 h and with no significant deterioration after 100 charge/discharge cycles. The capacity of InP/ZnS QDs was supposedly enhanced thanks to the quantum well-like band structure given by the core-shell geometry. The same was observed for CdSe/ZnSe core-shell particles.^[60] All-inorganic perovskite CsPbBr_3 QDs were also investigated in more than one instance for TBM device fabrication. These robust particles exhibit high photogenerated carriers' lifetimes, which are dramatically enhanced when coupled with a pentacene organic hole transport layer.^[55,60] As soon as excitons are generated, holes are transferred to pentacene due to its high energy HOMO and a sudden change in I_{DS} is observed, indicative of successful optical writing. The material was responsive under a range of different wavelengths, although the highest ON/OFF ratio was obtained at 365 nm, with continuous irradiation for 30 s (Figure 6c), indicating a still quite low R_{PC} for fast switching. Nevertheless, charges were successfully stored for at least 2.5 h. CsPbBr_3 QDs were also applied in memory devices as hole-storing particles.^[61] Other active layer materials, including

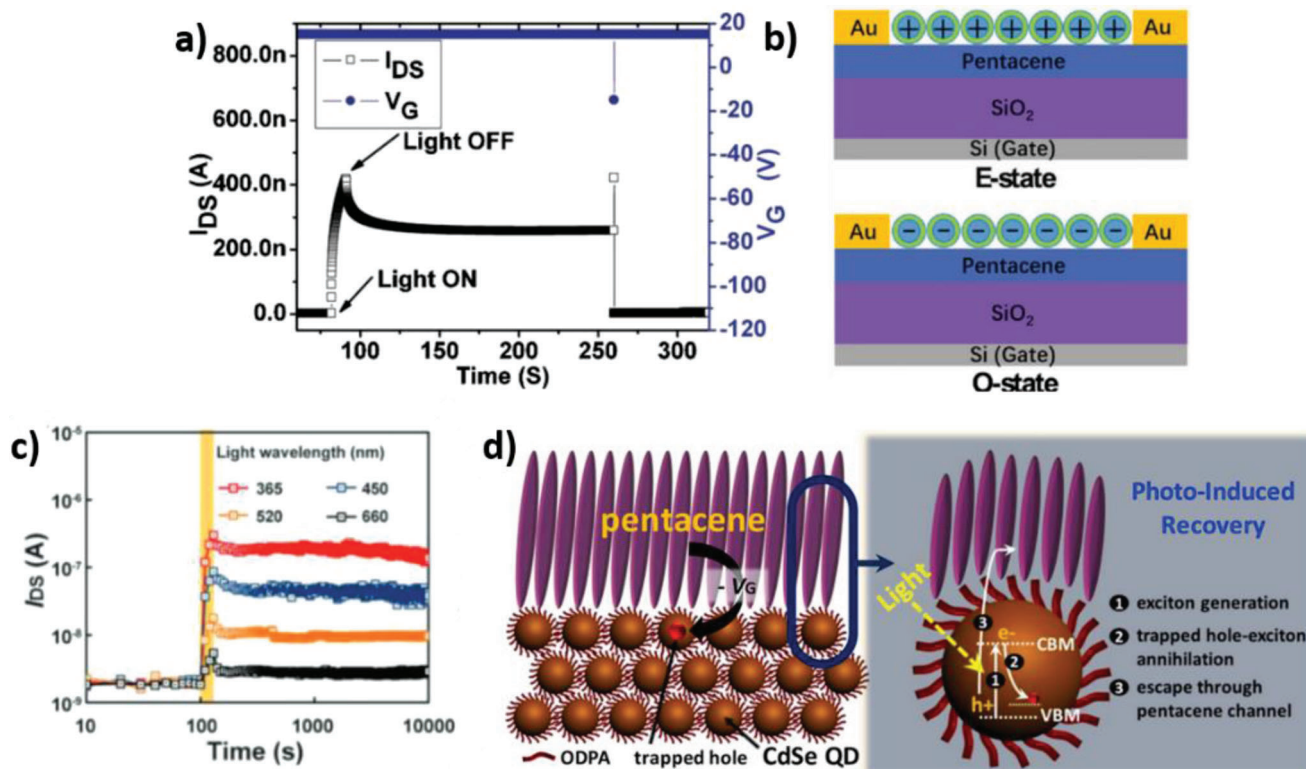


Figure 6. a) Optical writing and electrical erasing in the P3HT/CdSeQD device. Reproduced with permission.^[56] Copyright 2008. AIP Publishing. b) Scheme of the InP/ZnS QD-based device in its optically written (O) and electrically erased (E) states. Reproduced with permission.^[59] Copyright 2021. John Wiley & Sons. c) I_{DS} variation upon 30 s illumination of CsPbBr₃ QD-based device. Reproduced with permission.^[55] Copyright 2018. John Wiley & Sons. d) Scheme of the enhanced hole transfer from CdSe QDs to pentacene layer through organic ligands. Reproduced with permission.^[63] Copyright 2018. American Chemical Society.

graphene QDs and borophene/ZnO heterojunction were also investigated.^[62] Careful nanoparticle engineering can improve the performance of non-volatile memory devices. For example, CdSe QDs were capped with different organic ligands, with an outstanding enhancement of hole transfer to a conductive pentacene layer and, in turn, higher capacity (up to 26.7 nF cm⁻²) (Figure 6d).^[63] For some of the investigated ligands, light-driven state switching only required 1 s of illumination.

Information storage can also be accomplished by means of relatively new memristive devices, or memristors.^[64] Memristors are electrical components that keep memory of voltage and current applied to them in the form of a built-in, non-volatile resistance.^[65] Such components were first theoretically described by L. Chua in 1971, who speculated—purely on the basis of symmetry arguments—that a fourth circuit component should exist along with the well-known resistor, capacitor, and inductor.^[66] However, the first actual fabrication of a memristor only came out in 2008.^[67] Since then, a full research area on resistive switching (RS) memory devices has been developed.^[68,69] The general concept of a memristor is illustrated in Figure 7. The configuration includes a semiconducting or insulating material sandwiched between two conducting electrodes. The area enclosed by the electrodes possesses a doped and undoped region, with variable extension across its width (Figure 7a). The doped and undoped regions exhibit lower and higher resistance, respectively. If the width of the doped region (w) covers the total width of the mate-

rial (D), the device is in its low resistance state (LRS). Conversely, if the undoped region dominates, a high resistance state (HRS) is obtained. The w/D ratio can be changed by applying a voltage between the two metallic electrodes. Interestingly, current–voltage curves for such devices exhibit hysteresis, which is precisely what makes them memory devices (Figure 7b).^[69,70] In bipolar RS devices, information is written by sweeping a positive (SET) voltage, while it is erased with a negative sweep (RESET). During the SET process, a sudden decrease in resistance is observed at a critical switching potential (HRS to LRS switching) because of the formation of a conductive bridge, corresponding to a fully doped region. The LRS is retained unless a sufficiently high negative voltage is applied to break the conductive bridge and restore the fully undoped configuration. Different doping mechanisms can be identified, but all of them are ultimately based on the migration of charges between the two electrodes as a result of an applied electric field. The extension of the conductive bridge, consisting of either a metallic filament or the accumulation of positively charged vacancies, corresponds to the width w (Figure 7c).^[68,69,71] While charge leakage constitutes a major problem with the progressive miniaturization of TBM devices, this is not the case for RS technologies, which are not charge-based memories. Such property is considered to be the major advantage of RS devices.

The application of materials with optoelectronic properties in RS devices has been scarcely investigated. Again, different mechanisms for light-assisted memory storage in memristors can be

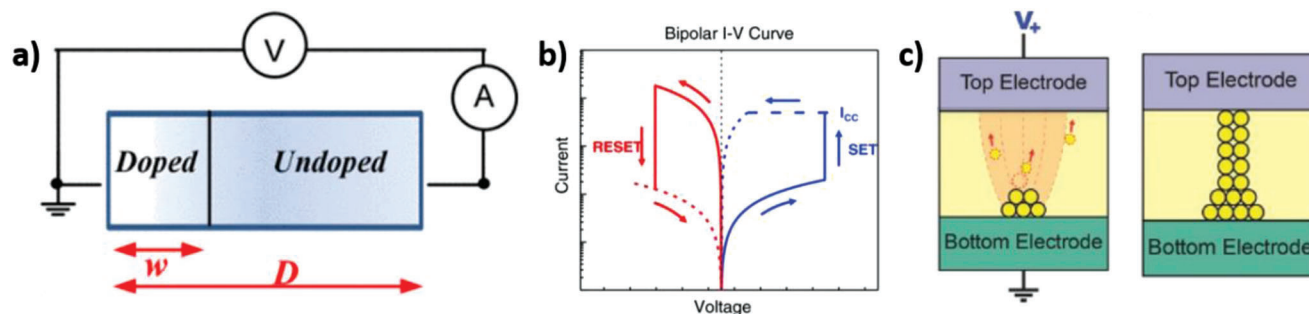


Figure 7. a) General scheme of a memristor. Reproduced with permission.^[72] Copyright 2009. IEEE. b) Typical I–V curve of a bipolar resistive switching device. c) Generation of a conductive bridge (SET process) of oxygen vacancies resulting from the migration of O^{2-} charges in oxide-based RS devices under the applied electric field. Reproduced with permission.^[69] Copyright 2017. John Wiley & Sons.

discussed.^[73] In particular, charge-storing semiconductors can improve memristors through photogating. Photogating consists of enhancing the electric field in the active region of the device by the light-driven accumulation of charges.^[74] A build-up of charges generated by light replaces the need for high SET voltages, significantly reducing electrical power consumption.^[71] As for TBM devices, QDs are the dominant photoactive materials found in photomemristors. Wang and co-workers fabricated a $CsPbBr_3$ QD-based RS device,^[75] while Lv et al. proposed a carbon dots-silk protein composite.^[76] In both cases, the SET and RESET switching voltages were shifted by 1.0–1.6 V to lower and higher values, respectively, when the irradiance of UV (365 nm) was increased up to 0.15 mW cm^{-2} . The devices exhibited good retention and endurance. In particular, the $CsPbBr_3$ perovskite-based maintained an ON/OFF current ratio for > 100 h and after more than 5000 SET-RESET cycles. The authors proposed that the conductive channel formed by the migration of Br^- toward the anode, leaving V_{Br^+} vacancies in the active material. In general, photoaccumulation of charges in QDs is supposed to enhance the mobility of ions via the photogate effect or to increase the conductivity itself because of the generated charge separation.^[73] Nevertheless, the relevance of these studies to semiconductor photocharging is still under debate. Indeed, several works on photo-tuned RS devices point toward a photovoltage rather than a photo-

gating effect, in which excited carriers are transferred toward the electrodes—with an increase in conductivity—rather than trapped in the nanoparticles. This scenario is probably the most relevant for a variety of other reported devices.^[77]

With reference to memory-storage technologies for authentication purposes, Fang et al. reported an original application of polymeric carbon nitrides in anticounterfeiting devices based on photochromism.^[78] Their design consisted of a K-PHI/poly(vinyl alcohol)(PVA) film with randomly distributed particles that could change color upon irradiation. The random distribution of K-PHI particles is inherent to the fabrication process, which makes the material a physical unclonable function (PUF). Unlike conventional anticounterfeiting labels made by reproducible coding processes, PUFs cannot be accurately replicated, thus preventing cloning.^[79] Blending K-PHI with PVA suppresses electron scavenging by atmospheric oxygen, therefore different colors and persistence of the photochromic effect can be obtained by varying the K-PHI/PVA ratio in the fabricated film (**Figure 8**). The color, visible to the naked eye, constitutes the first level of safety, while the exact pattern of K-PHI particles is a further level that can be detected by a customized authentication program. The labels were easily verified by collecting pictures on a smartphone equipped with a portable objective. The authors demonstrated that the program could distinguish real from fake labels and that

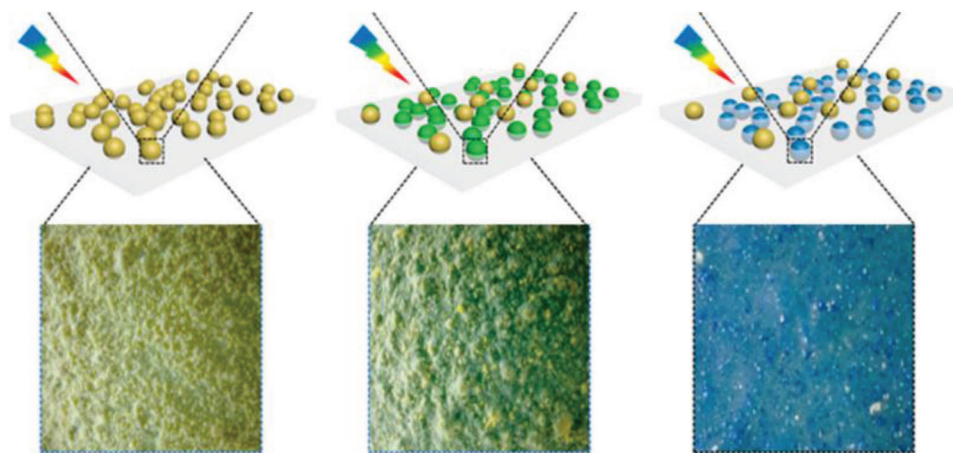


Figure 8. Scheme and pictures of irradiated anticounterfeiting labels made of PVA films of randomly distributed K-PHI particles with decreasing K-PHI/PVA ratio from left to right. Reproduced with permission.^[78] Copyright 2022. American Chemical Society.

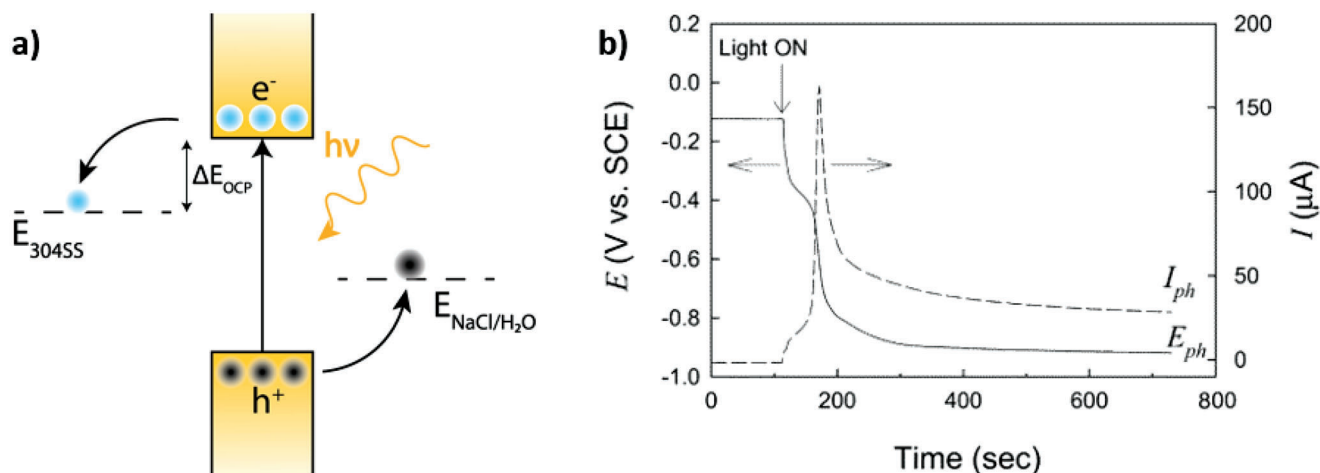


Figure 9. a) Band structure of the ideal semiconductor for photocathodic protection. The corrosion potential of 304 stainless steel and the redox potential of a NaCl/H₂O solution are illustrated as examples. b) The evolution of steel open circuit voltage and photocurrent upon UV illumination of an electrically wired TiO₂ photoanode. Reproduced with permission.^[86] Copyright 2002. American Chemical Society.

the verification was not influenced by the brightness or saturation of the picture. It is important to note that the readout needed to be completed within 17 min after 1 min of UV irradiation, because of the gradual decay of photochromism induced by oxygen. This limitation could be overcome in the future using particles with low discharging rates. In that sense, PUF anticounterfeiting devices made of bigger particles might exhibit prolonged photochromism, so that labels would not need frequent irradiation for their readout.

5. Photocathodic Protection for Anti-Corrosion

The corrosion of metals or alloys is a long-standing issue for the construction industry.^[80,81] In particular, the oxidation of type 304 stainless steel (SS) is of high concern to naval engineering.^[81,82] Corrosion is usually tackled by cathodic protection, which consists of either the application of an external current to prevent the oxidation and dissolution of the metal or the installation of sacrificial anodes that are oxidized instead of the working material.^[83] Photoelectrochemical (PEC) cathodic protection has emerged in the past decades as an environmentally friendly and efficient alternative to traditional techniques. In PEC systems, a cathodic current transferred to the active material is generated by light. This process not only reduces the costs of an external electrical supply but also avoids the consumption of the protecting material at the photoelectrode, which essentially plays the role of a catalyst. Conversely, sacrificial anodes like Zn and Mg have a limited lifetime, release metal ions into the environment upon oxidation, and need to be replaced regularly.^[84,85] Cathodic protection is fulfilled if the rate of photogenerated electron transfer to the metal is faster than the corroding reaction. Usually, such a requirement is easy to meet given that corrosion is inherently slow. In fact, the ideal photoelectrode should keep a reservoir of electrons as long as possible, so that they can be delivered on demand. Hence, semiconductor photocharging can definitely contribute to this field. While quantum yield and solar-to-chemical energy conversion are crucial in photoelectrodes for water splitting, prolonged activity in the dark is more important in photoca-

thodic protection.^[83] Moreover, the redox or CB edge potential of the photoactive material should be more negative than the corrosion potential of the protected material. The difference between them at open circuit conditions (ΔE_{OCP}) should be as high as possible and maintained for as long as possible. On the other hand, holes are transferred to a substrate that is oxidized, which ideally should be a seawater-mimicking NaCl/H₂O solution. The redox potential of this electron-donating substrate should be more negative than the VB edge of the semiconductor. The more negative, the higher the driving force for hole scavenging (Figure 9a).

The first light-driven cathodic protection was reported in 1995 and consisted of sol-gel TiO₂ coated on copper. The coating limited the oxidation of the metal when illuminated under a Hg lamp, which was confirmed through glow discharge spectroscopy.^[87] The field was then pioneered by Park and co-workers.^[86,88] They observed that when a UV-illuminated TiO₂ photoanode was wired to steel, this maintained a shiny appearance and its open circuit potential dropped by ≈ 0.6 V and a photocurrent spiked and reached equilibration (Figure 9b).^[86] The potential drop indicates the electron injection from the photoanode and is the main experimental evidence for the assessment of photocathodic protection. The authors also compared different hole scavengers. Unsurprisingly, water resulted in the lowest photocurrent, because of the sluggish kinetics of water oxidation. Above all, the work insisted that the major limitation of the technology was its inactivity in the dark. Indeed, electron transfer from the semiconductor was not enough to compensate for the dark corrosion current. The authors concluded by proposing a design of a TiO₂ photoanode coupled to a rechargeable battery for night hours (Figure 10a). Such architecture is admittedly cumbersome and costly, which is why electron-storing semiconductors are extremely promising in this area. Although several examples of Ti-based semiconductors for light-assisted anti-corrosion followed,^[89] the interest in intrinsic energy-storing photoanodes for cathodic protection has flourished in the past few years.^[85,90] Actually, the first example of energy-storing photoanodes for anti-corrosion was proposed as early as 2001.^[91] There, when stainless steel was coated with a TiO₂/WO₃ composite, the open circuit

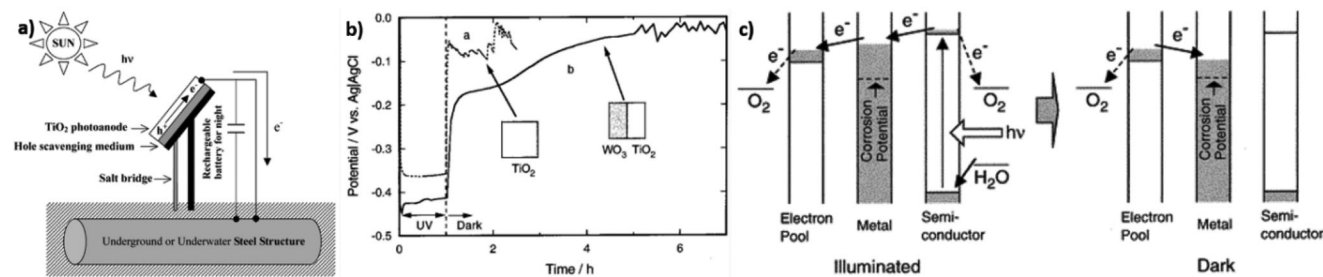


Figure 10. a) Illustration of the photocathodic protection design coupled to a rechargeable battery for prolonged anti-corrosion activity in the dark proposed by Park et al. Reproduced with permission.^[86] Copyright 2002. American Chemical Society. b) OCP of stainless steel coated with TiO₂ or a TiO₂/WO₃ heterojunction during and after UV irradiation. c) General mechanism of the “electron pool” heterojunction strategy for photocathodic protection with energy storage. Reproduced with permission.^[91] Copyright 2001. American Chemical Society.

potential was maintained < -0.1 V versus Ag/AgCl—considered as the “corrosion potential” for 304 SS—for > 6 h (Figure 10b). Further contributions from Park et al. revealed that the rate of discharging was proportional to WO₃ content,^[92] and that the same material successfully prevented corrosion in a photoanode.^[93] Interestingly, they showed that the discharging time increased up to 22 h if the anode was irradiated for longer times, even if the OCP reached a saturation of -0.6 V versus Ag/AgCl within the first 4 h. The result probably indicates that at saturation electron transfer to the cathode becomes the limiting process, while electrons are still trapped. TiO₂/WO₃ heterojunctions are the first choice when it comes to photocathodic protection with long-term activity in the dark.^[85,90] In general, the heterojunction approach consists of a light-absorbing semiconductor (TiO₂ being the state of the art) coupled to an electron pool. Electrons are photogenerated in the former and then transferred to the latter when they reside for a sufficiently long time (Figure 10c). For this design to work, the electron-storing material should have i) CB at more positive potentials than the CB of the photoexcited semiconductor and ii) trapping sites for electrons. WO₃ perfectly satisfies both conditions. In particular, it is easily converted to tungsten bronzes thanks to its ability to accommodate monovalent metal cations through intercalation, according to the reaction $\text{WO}_3 + \text{M}^+ + \text{x}e^- \rightarrow \text{M}_x\text{WO}_3$.^[13,94] Thus, electrons are temporarily stored at W centers with concomitant W(VI)-to-W(V) reduction. Electrochemical studies confirmed that photogenerated electrons are swiftly transferred from TiO₂ to WO₃ and subsequently reside in the latter with slow discharge to steel in the dark.^[93] Numerous reports of energy-storing TiO₂/WO₃ heterojunction for anti-corrosion have been reported,^[95–101] as well as equivalent structures with bronze formation reaction based on MoO₃,^[102] SnO₂,^[103–106] and V₂O₅.^[107]

Further approaches on the electron pools involved Mn–Ti,^[108] In–Ti,^[109–111] Ni–Ti,^[112,113] Bi–Ti,^[114–116] Ce–Ti,^[117] Mn–Ti,^[108] Ag–Ti,^[118] SrTiO₃–TiO₂.^[119] One of the best-performing photoanode for cathodic protection consisted of a Fe-doped TiO₂ array of nanotubes, reported by Li et al.^[120] The doping extended the absorption from the UV to the full visible region and led to outstanding stored charge longevity. After only 4 min of illumination under a Xe lamp, the OCP of 304 SS dropped by 0.22 V—well below the corroding potential—and was stable for > 2 h. Although no clear mechanistic studies were performed, they speculated that photogenerated electrons could be stored at Fe^{III} centers via d–d transition or charge transfer disproportion ($\text{Fe}^{3+} + \text{Fe}^{3+} \rightarrow$

$\text{Fe}^{4+} + \text{Fe}^{2+}$). The result is particularly meaningful for its very high $R_{\text{PC}}/R_{\text{DC}}$ ratio. A similar auxiliary function of Fe was also observed for Fe-doped TiO₂ films, which exhibited corrosion protection for > 12 h in the dark after 1 h illumination, and was simply attributed to an extended carrier lifetime.^[121] In addition to those bulk heterojunctions, the application of QD nanoparticles including ZnS, CdS, CdSe, CdTe, and SnO₂ adsorbed on TiO₂ was also explored. Generally, very good results were obtained thanks to the charge-storing properties of QDs, functioning as electron pools.^[122–127] These materials achieved among the best prolonged cathodic protection in the dark with excellent OPC shifts and $R_{\text{PC}}/R_{\text{DC}}$ ratio (Table 2), confirming QDs as state-of-the-art charge-storing semiconductors. In a few instances, introducing 2D carbon layers proved to be beneficial for enhanced charge separation and storage. Reduced graphene oxide (RGO) inserted in a WO₃/TiO₂ heterojunction improved the OCP shift—that is, the total accumulated charges—likely because of its high contact area with TiO₂ and its low Fermi energy.^[101] The same was demonstrated for SnO₂/TiO₂^[106] and ZnIn₂S₄/TiO₂.^[110] The strategy was also investigated by Zhang and co-workers to construct an organic/inorganic heterojunction.^[128] The authors deposited polyaniline (PANI) on a TiO₂ photoanode. PANI is a polymer containing quinonoid units that can be photoreduced by electron donors, accumulating electrons under illumination. When light is turned off, the units are oxidized again, and electrons are released (Figure 11b). Although PANI itself is not capable of accumulating electrons, a remnant photocurrent was observed when coupled to graphene (Figure 11a,c). Graphene is supposed to temporarily store electrons released from PANI thanks to the extended π interaction with the aromatic moieties in the polymer. Indeed, a graphene-free PANI–TiO₂ heterojunction could not sustain any current in the dark (Figure 11c). Although no experiment on the long-term shift of steel’s OCP was performed, the result spawns interest in organic polymer/graphene composites as photoactive electron-storing material.

It should be reminded that such architectures do not strictly belong to the category of photochargeable semiconductors, since they rely on a two-step charging-storing process. Instead, they are more correctly referred to as energy-storing heterojunctions. TiO₂ has been the dominating—if not exclusive—active component so far. This gives rise to two main limitations: i) the need to fabricate band-matched multi-component materials and ii) useful light is restricted to the UV or high energy visible region. The ideal active material for day-night anti-corroding photoanodes

Table 2. Summary of energy-storing materials for photocathodic protection.

Category ^{a)}	Material	Irradiation source	SS OCP drop [mV]	Longest protection time [h]	R _{PC} /R _{DC}	Reference
Heterojunction with TiO ₂						
W-based	WO ₃ /TiO ₂	Hg/Xe lamp (>365 nm)	≈ 100	5	5	[91]
	WO ₃ /TiO ₂	Hg/Xe lamp	550	6	2	[92]
	WO ₃ /TiO ₂	AM-1.5	450	12	15.6	[93]
	ZnS-Bi ₂ S ₃ /TiO ₂ /WO ₃	Xe lamp	100	2	16	[95]
	WO ₃ /TiO ₂	Hg lamp	215	6	6	[96]
	WO ₃ /TiO ₂	Xe lamp	250	9	12	[97]
	WO ₃ /TiO ₂	Xe lamp	180	27	13.2	[98]
Mo-based	MoO ₃ /TiO ₂	Xe lamp	200	15	3	[102]
Sn-based	Ag/SnO ₂ /TiO ₂	Xe lamp (> 400 nm)	200	7.6	4.2	[104]
	SnO ₂ /TiO ₂	Xe lamp	200	16	5.3	[105]
V-based	TiO ₂ -V ₂ O ₅	Hg lamp (365 nm)	60	6	6	[107]
	BiVO ₄ /TiO ₂	Xe lamp	90	20	5	[114]
Mn-based	MnS/TiO ₂	Xe lamp	80	5	1	[108]
Ni-based	NiO ₂ /TiO ₂	Xe lamp	240	5	6	[112]
Bi-based	β-Bi ₂ O ₃ /TiO ₂	Xe lamp	50	15	7.5	[115]
Ce-based	CeO ₂ /SrTiO ₃	Xe lamp	10	7	6.3	[117]
Ag-based	Ag/graphene/TiO ₂	Xe lamp	310	22	4.9	[118]
Ti-based	SrTiO ₃ /TiO ₂	Xe lamp	80	16	8	[119]
QD-based	ZnS/CdSe/CdS/TiO ₂	Xe lamp	300	47	9.4	[122]
	CdTe/ZnS/ TiO ₂	Xe lamp	250	13	3.7	[123]
	ZnS/CdS@TiO ₂	Xe lamp	220	5	2	[124]
	CdSe/RGO/TiO ₂	Xe lamp	400	24	4.8	[125]
	CdTe/graphene/TiO ₂	Xe lamp	280	8.5	3.7	[126]
PCN-based	ZnIn ₂ S ₄ /SnO ₂ /TiO ₂	Xe lamp (> 400 nm)	130	10	10	[127]
	PCN/TiO ₂	Xe lamp	140	2	1	[129]
TiO ₂ -free	PCN (loose film)	Xe lamp	210	0.85	0.5	[132]
	Co ₃ O ₄ /CdS	Xe lamp	120	11	35	[135]

^{a)} Only materials yielding at least 1 h protection in the dark were included.

should be intrinsically charge-storing and visible light-absorbing. Polymeric carbon nitrides respond well to both demands, given their relatively low bandgap (≈ 2.7 eV) and proven charge-storing properties explored in the context of dark photocatalysis.^[17] PCN for photocathodic protection have been already investigated to a good extent. Although the first examples still focused on PCN/TiO₂ heterojunctions,^[129] more recent works have shown the potential of all-PCN photoanodes for the prolonged anti-corrosion of stainless steel. Yuyu and co-workers first reported a PCN-only photoanode with good anti-corrosion properties under intermittent illumination with both white and visible light.^[130] Jing et al. doped PCN by the polycondensation of urea in a KI solution.^[131] The n-doped semiconductor downshifted the OPC of a coupled 316L stainless steel electrode under illumination, with a slow recovery in the dark indicating marginal charge storage. Conversely, corrosion was accelerated using the undoped material. The work reiterates the importance of a sufficiently negative conduction band in materials used for photocathodic pro-

tection. Li et al. proposed the most promising solution based on a PCN photoanode, where electron recombination was suppressed in a polymeric carbon nitride with a loose morphology (**Figure 12a**).^[132] Compact carbon nitride films (CCNF) were first prepared on fluorine-doped tin oxide (FTO) from dicyandiamide by thermal vapor deposition. Then, exfoliated structures were achieved by thermal annealing at 600°C for 10 and 40 min, yielding transition carbon nitride film (TCNF) and loose carbon nitride film (LCNF). Exfoliation is expected to occur because of the release of CO₂ and NH₃ at annealing temperatures. When the photoanode was coupled to Q235 carbon steel and irradiated under white light for 1.7 h, the OCP of steel shifted from its corrosion value from -0.67 to -0.88 V versus Ag/AgCl with LCNF, while CCNF and TCNF yielded lower shifts (**Figure 12b**). Discharge to the original corrosion potential occurred in 0.85 h for LCNF, and in a few seconds for CCNF (**Figure 12c**). The results indicate that LCNF have both a higher electron storage capacity and slower discharge rate. The authors attributed the higher

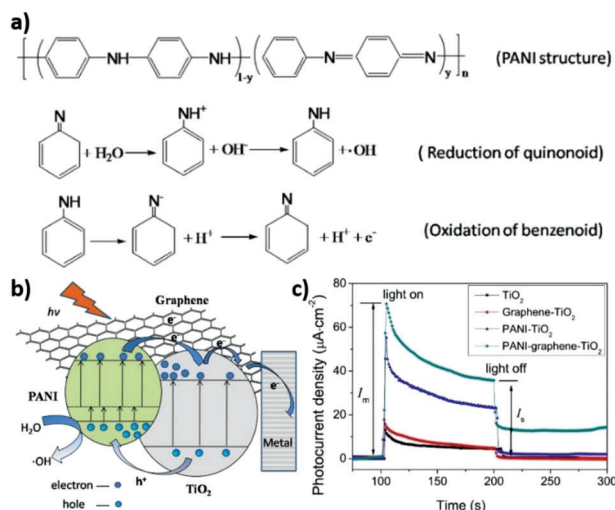


Figure 11. a) Illustration of the PANI-graphene-TiO₂-metal heterojunction. b) Structure of PANI along with reduction of quinonoid units under illumination and oxidation in the dark. c) Photocurrent responses of different combinations of PANI/graphene/TiO₂ heterojunction on a metal steel electrode under light and dark conditions. Reproduced with permission.^[128] Copyright 2017. Elsevier.

energy-storage efficiency to the faster kinetics of Na⁺ counterions transfer between the PCN sheets in the expanded morphology, which is consistent with trends shown by photochargeable semiconductors in different fields.^[5] Although the R_{PC}/R_{DC} ratio is still very low compared to the state-of-the-art TiO₂-based photoanodes (Table 2), the work opens a new field of application of energy-storing carbon nitrides other than dark photocatalysis. It should be noted that such a negative shift in potential was only possible in the presence of 0.1 M Na₂S as a sacrificial electron donor, which is clearly a non-realistic scenario for anti-corrosion in seawater. More applications of all-carbon nitride materials in light-driven anti-corrosion were explored, but none of those exhibited significant energy storage.^[133]

More reports on TiO₂-free composites for photocathodic protection have been released, with the most promising still relying on the WO₃-based electron pool strategy.^[134] Recently, the first Co-based photoanode with energy-storing capacity for cathodic protection was reported.^[135] The material consisted of a Co₃O₄/CdS bilayer film. Although the authors attributed the excellent charge-storing properties to the nanoporous structure, it is quite evident that electrons are in fact stored in CdS as in other QD-based structures. An OPC at the 304 SS counter electrode well below the corrosion potential was maintained for 11 h after only ≈ 15 min irradiation, giving the highest discharge/charge time ever achieved. It is worth mentioning that many of the materials discussed in this section possessed a highly ordered structure. In particular, for most TiO₂-based photoanodes the main semiconductor is fabricated in the form of nanotubes or other vertical arrays on the electrode.^[108,113–116,118,125–127,136] It is believed that such morphology favors the oriented transfer of electrons, thus suppressing carrier recombination.^[85,137] Alternatively, the increased surface area might provide more charge-trapping sites. Nevertheless, no robust mechanistic study was ever reported to support this hypothesis, and strategies based on unique struc-

tures of photochargeable materials seem hard to reproduce. Instead, the role of heterojunctions in carrier separation and storage is much better understood and reliable.

Much work has already been done on light-driven materials that can give rise to the first real “non-sacrificial” anodes. Not enough attention has been dedicated to the long-term action of these devices, which can potentially prevent steel corrosion 24 h a day for the whole lifetime of a ship. More effort on this aspect is needed, and we propose the discharge/charge time ratio (R_{PC}/R_{DC}) as a key figure of merit to evaluate day-night anti-corrosion activity. Despite the aroused interest in energy-storing materials for this application, critical constraints still prevent their real-world application. In particular, three major challenges need to be addressed to develop the optimal charge-storing materials for photocathodic protection: i) extend absorbing properties to visible light, ii) replace the need for hole scavengers, and iii) induce a sufficiently high OCP drop. The first point has already been covered in part. The best solutions to move from UV-absorbing TiO₂ are coupling with low bandgap semiconductors (e.g., WO₃), light-absorbing QDs, or PCN. However, studies on photoelectrochemical anti-corrosion still heavily rely on sacrificial hole scavengers on the anodic compartment. In particular, a Na₂S/NaOH solution is the most common electrolyte, with sulfide ions acting as electron donors in a basic environment to prevent hydrolysis. Ideally, abundant water with 3.5 wt. % NaCl should be the hole scavenger. While water oxidation is kinetically sluggish, oxidation of chloride anion is more facile. Still, very few reports in such electrolyte have been reported so far.^[109,138] This is especially relevant to semiconductors having low VB potentials like PCN.^[85,129–132] A possible solution would be coupling the photoactive material with a hole-scavenging semiconductor featuring a more positive VB edge, as it was shown in a TiO₂/Co(OH)₂ composite.^[138] Finally, the OCP provided by most of the systems revised here might not be low enough for efficient prevention of steel corrosion in marine environments. More specifically, several organizations including the National Association of Corrosion Engineers (NACE) agree that for efficient protection from corrosion, the potential of steel should be maintained < −0.8 V versus Ag/AgCl in aerated seawater, or −0.9 V versus Ag/AgCl in anaerobic conditions like mud water.^[139] To achieve such low numbers, semiconductors with very negative CB edge are needed. PCN are good candidates in this sense, with a CB lying at potentials more negative than ≈ −1.0 V versus Ag/AgCl.^[12,140] Of course, PCN should be coupled in a plausible Z-scheme with a more oxidative semiconductor to enable water oxidation. The stability of PCN on electrodes also needs to be improved.^[141] None of the reported energy-storing devices for photocathodic protection can shift the OCP of steel down < −0.8 V versus Ag/AgCl in the dark, but different examples of heterojunctions with TiO₂ can meet that requirement under illumination.^[100,104,112,118,122,124,125,127,135] For these materials, charge accumulation might still be relevant to prolong the lifetime of steel, where corrosion could be reasonably prevented during the day and sufficiently slowed down at night.

6. Sensors and Analytical Devices

The most evident manifestation of photocharging is photochromism. Photocharging was first realized when researchers

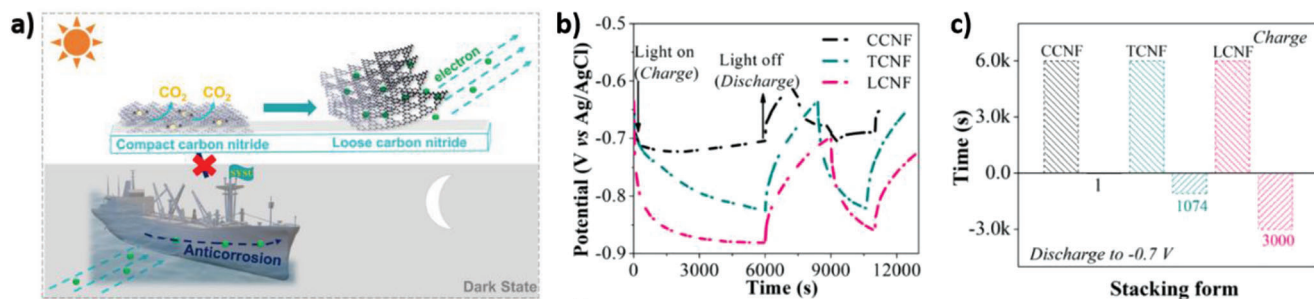


Figure 12. a) Illustration of the expansion of polymeric carbon nitriles into a loose morphology and its application for decoupled daytime energy storage and slow discharge at night. b) OCP shifts of a Q235 carbon steel electrode coupled to a photoanode coated with carbon nitriles of different morphologies under illumination followed by dark conditions. c) Discharge time for the Q235 carbon steel electrode to recover a -0.7 V versus Ag/AgCl potential after 6000 s of photocharging using different morphologies of carbon nitride. Reproduced with permission.^[132] Copyright 2020. American Chemical Society.

observed that suspensions of TiO₂ nanoparticles turned blue when irradiated under UV light.^[7,20] Photochromism was also the first clue of the photocharging properties of poly (heptazine imides).^[17,142] Such semiconductors need to operate in oxygen-free conditions for most of their applications based on photocharging, given that O₂ is a strong electron scavenger. Nevertheless, what is a hurdle under certain circumstances can be turned into an opportunity to detect oxygen, which is an analyte of great relevance to biomedicine, the food industry, and the preservation of historical artifacts.^[143] Han and co-workers have recently proposed a simple colorimetric method for oxygen sensing based on the reversible color switching of PCN.^[144] An aqueous suspension of the photoactive material was first charged via illumination with a Xe lamp in an oxygen-free atmosphere using TEOA as a hole scavenger, which was accompanied by a stark color change visible to the naked eye. Then, the introduction of oxygen in the suspension restored the original appearance in the discharging process (Figure 13a). The reflection of the suspension increased roughly linearly with concentrations of the gas <10% vol (Figure 13b,c).

The authors compared the photochromic effect in pristine (CN), potassium (CN-K), and sodium (CN-Na) doped polymeric carbon nitriles, obtained from the calcination of urea alone or mixed with KI or NaI. No evident photochromism occurred in CN. CN-K and CN-Na suspensions acquired different colors (blue and brown, respectively) upon irradiation (Figure 13a), suggesting that they would perform as oxygen sensors in different analytical ranges, as demonstrated in Figure 13c. DFT studies suggested that the charge separation was enhanced in ionic carbon nitriles, with electrons preferentially trapped on edge C≡N and C=O groups. Elemental analysis, X-ray photoemission (XPS) spectroscopy, and ¹³C solid state nuclear magnetic resonance (NMR) spectroscopy revealed a higher concentration of C=O groups on CN-Na compared with CN-K. Accordingly, when the suspensions were bubbled with an excess of oxygen after photocharging, CN-Na consumed more O₂ than CN-K, indicating a higher electron storage capacity. The electron storage capacity, hence, the analytical range, could be easily tuned by varying the Na/K ratio in the synthetic procedure. The charge/discharge cycle could be repeated > 100 times, with no depletion of

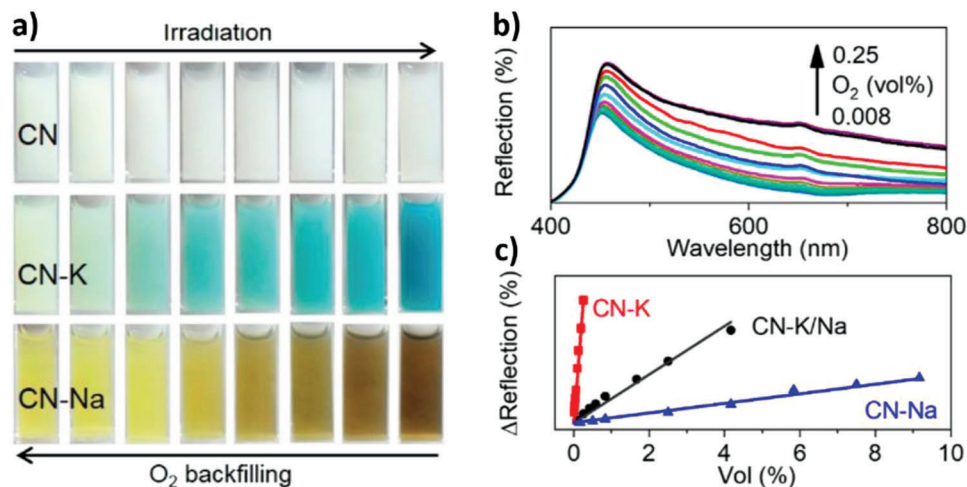


Figure 13. a) Color change observed upon irradiation (left to right) and oxygen bubbling (right to left) of CN, CN-K, and CN-Na aqueous suspensions. b) Reflection spectra of a CN-K aqueous suspension at different concentrations of O₂. c) Reflection-O₂ concentration calibration curves of CN-K, CN-Na, and a sample synthesized with an equimolar mixture of KI and NaI (CN-K/Na). Reproduced with permission.^[144] Copyright 2022. American Chemical Society.

electron storage capacity and good reproducibility of the quantified oxygen concentration. The authors also showed that the method reaches lower limits of detection than most conventional oxygen sensors. However, the process is not limited to oxygen sensing and a variety of electron scavenging analytes (e.g., persulfate) may be considered in the future. Overall, reversibility is the added value of the colorimetric method based on carbon nitride photochromism. Indeed, many colorimetric analytical protocols rely on inherently irreversible chemical reactions, like in the routinely used pH paper indicators. Conversely, photochargeable semiconductors are swiftly charged with light without damaging their chemical structure in most cases, akin to secondary batteries. Despite this work being the only report on oxygen sensing based on photoinduced electron storage, the ease of operation together with the vast library of charge-storing semiconductors is expected to inspire new designs. Other colorimetric approaches based on photocharging might be explored. For example, core-shell Ag@TiO₂ nanoparticles exhibited >20 nm blueshift of the plasmon resonance band arising from the Ag core when irradiated under UV for 1 min.^[145] The band redshifted in the presence of an electron scavenger. Although the authors did not propose any analytical application, it is evident that the plasmon shift can be a key signal to quantify electron scavengers in solution. The particles should be engineered to operate in a meaningful and large enough analytical range.

As described in the previous paragraphs, electron accumulation in semiconductors can be greatly enhanced by the presence of hole scavengers. Thus, for certain materials and conditions, a relationship between the total amount of stored electrons (δ_{\max}) and the concentration of hole scavenger (C_s) can be found. Such dependence precisely enables quantifying electron-donating analytes. Gouder et al. reported one of the most comprehensive studies on the application of PHIs in optoelectronics for small molecule sensing in aqueous media.^[146] K-PHI was investigated for its remarkable visible light absorbance and charge-storing capacity.^[17,40] In the workflow proposed, K-PHI is first photocharged under simulated solar light, then mixed with an aqueous solution of the analyte glucose. Different readout methods were discussed and compared. In a preliminary step, the authors demonstrated that glucose can be easily quantified in situ by measuring the generated photocurrent in a photoelectrochemical cell (PEC), where K-PHI was adsorbed on the working electrode. Indeed, the measurement of photocurrent is a routine procedure in PEC devices for catalytic purposes, from which product yield and faradic efficiency are determined.^[39,147] Nevertheless, the main goal of the work was to achieve time-delayed quantification, or “memory sensing”. Taking advantage of the prolonged charge accumulation in K-PHI, the work demonstrated that the semiconductor could keep memory of the concentration of the sampled analyte so that writing and reading steps could be time-separated (Figure 14a). K-PHI was either adsorbed on an FTO substrate and subsequently mounted in a three-electrode cell as a working electrode or dispersed in solution for electronics and spectroscopic readout, respectively. Different electrochemical methods were considered for the reading process, including potentiometric, impedimetric, and coulometric. In the first, glucose concentration was determined from the shift in the open circuit potential (OPC). Higher glucose concentration resulted in higher electron build-up in K-PHI, hence in more negative OPC

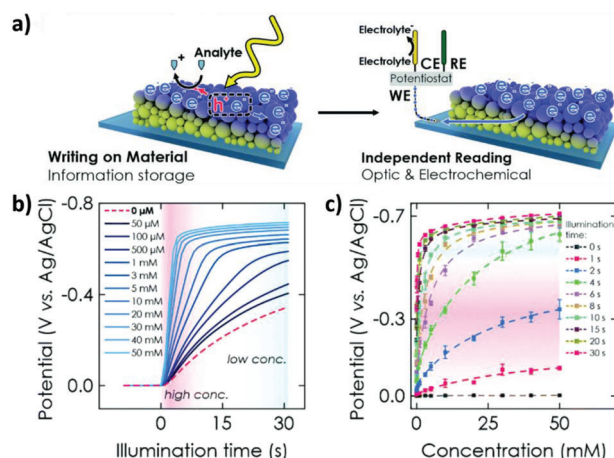


Figure 14. a) Schematic illustration of time-separated writing on K-PHI and reading of stored electrons proportional to the analyte concentration; b) OPC-illumination time curve measured at different glucose concentrations; c) OPC-glucose concentration curve measured at different illumination times. Reproduced with permission.^[146] Copyright 2022. Royal Society of Chemistry.

(Figure 14b). For impedimetric readout, the magnitude of the total impedance at a given frequency was determined by electrochemical impedance spectroscopy (EIS). Finally, the coulometric readout basically consisted in discharging K-PHI—that is, erasing the stored memory—by applying a strong positive bias. The total accumulated charge, proportional to glucose concentration, could be calculated as the integral of the $I-t$ discharge curve. It should be noted that this is a destructive readout, otherwise accumulated electrons persisted in K-PHI for at least 1 h. Colorimetric and fluorimetric methods based on color change of K-PHI aqueous suspensions upon photocharging were also proposed. These alternative methods are more relevant to in situ analysis of biological samples, for instance. All the readout methods summarized could sense glucose in a concentration window between 0.1 and 20 mM on average. Most interestingly, the authors showed that the analytical sensitivity could be easily customized by adjusting the irradiation time or intensity during the charging step. The higher the number of photons, the higher the number of stored electrons and, in turn, the sensitivity of the readout method. As an example, this concept was demonstrated for potentiometric sampling (Figure 14c). This work illustrates a simple design where customized analytical ranges are obtained by choosing appropriate irradiation doses. Interestingly, this is a rare example of an application that would benefit from low R_{PC} . In fact, if saturation is reached too fast, the analytical range shrinks dramatically. The sampling range can be extended with higher δ_{\max} . Low R_{DC} is needed to prevent electron leakage from the reaction of photocharged K-PHI with oxygen.

Finally, the electron-storing capacity of polymeric carbon nitrides also led to the first report of so-called “afterglow electrochemiluminescence”.^[148] Electrochemiluminescence (ECL) is a phenomenon often harnessed for analytical purposes. Briefly, an applied voltage generates excited species with separated charges that recombine with the emission of photons. The emission intensity is generally proportional to the concentration of the analyte, through many possible mechanisms. Light is

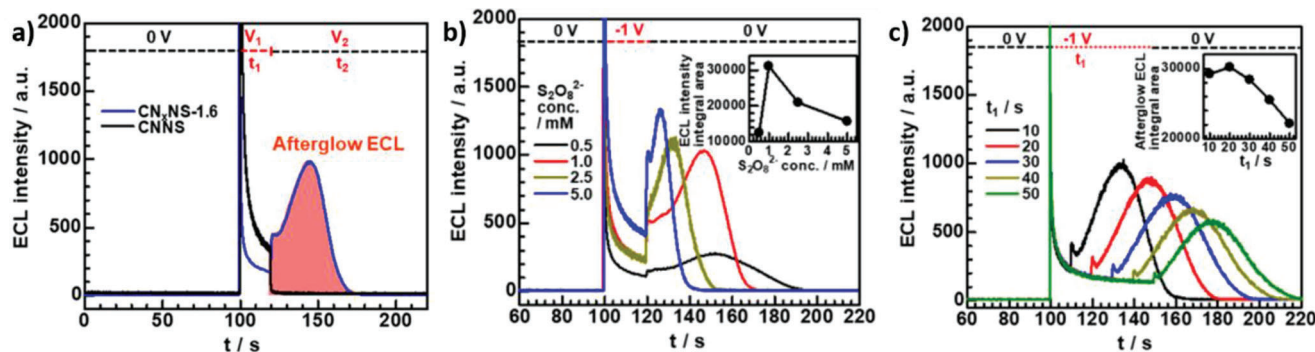


Figure 15. a) Afterglow ECL of $\text{CN}_x\text{NS-1.6}$ electrodes in 1 mM $\text{K}_2\text{S}_2\text{O}_8$ under an applied bias of 1.0 V versus Ag/AgCl (V_1) maintained for 20 s (t_1). b, c) Dependence of $\text{CN}_x\text{NS-1.6}$ total afterglow ECL on (b) concentration of $\text{K}_2\text{S}_2\text{O}_8$ and (c) t_1 . Reproduced with permission.^[148] Copyright 2023. American Chemical Society.

emitted as long as the potential is applied. “Afterglow” indicates a prolonged luminescence after removing the applied bias. The term is commonly used in the field of persistent phosphors, that is chemical species with long-lived phosphorescence. Such materials are extensively used in bio-imaging and are based on lanthanide ions.^[149] The use of PCN in ECL was first reported by Cheng et al.^[150] PCN emitted light centered at 470 nm (the typical fluorescence peak of carbon nitrides) when used as a working electrode with an applied bias < −0.1 V versus Ag/AgCl, in the presence of potassium persulfate ($\text{K}_2\text{S}_2\text{O}_8$) as electrolyte. In the proposed mechanism, electrons are transferred from the electrode to both PCN and $\text{S}_2\text{O}_8^{2-}$, generating the charged species $\text{PCN}^{\bullet-}$ (1) and $\text{SO}_4^{\bullet-}$ (2), respectively. The sulfate radical anion then transfers a hole to the valence band of $\text{PCN}^{\bullet-}$, generating the excited species PCN^* (3). Charge recombination with the emission of a photon terminates the process (4):



The method was tested for the detection of Cu^{2+} at the sub-nanomolar level since it was shown to quench the electrogenerated chemiluminescence. However, the role of Cu^{2+} was not discussed and luminescence was only investigated under constant applied bias. Building on the same mechanism, very recently Chen and co-workers showed that a nitrogen-deficient PCN electrode emitted light even for ≈ 1 min after the bias was removed.^[148] Carbon nitride modified with 1.6 g of potassium thiocyanate (KSCN) was investigated because of its higher density of defect states centered on dangling cyanamide moieties.^[151] The material in the form of nanosheets ($\text{CN}_x\text{NS-1.6}$) was deposited on a glassy carbon electrode. When a voltage of −1.0 V versus Ag/AgCl was applied in a 1 mM $\text{K}_2\text{S}_2\text{O}_8$ solution, light peaked at 455 nm was emitted. When the bias was applied for 20 s and switched off, luminescence initially increased and slowly decayed within 70 s (Figure 15a). Such afterglow ECL was not observed with unmodified carbon nitride nanosheets (CNNS),

suggesting that the emission in the dark could be attributed to stored charges on defect states in N-deficient $\text{CN}_x\text{NS-1.6}$. The authors probed how different parameters affected the afterglow lifetime. In particular, the total afterglow ECL decreased with $\text{K}_2\text{S}_2\text{O}_8$ concentrations below or above 1 mM (Figure 15b). Increasing the duration of applied bias (t_1) had the same effect (Figure 15c).

The results are rationalized according to the same mechanism described in Equations (1–4), with the addition of trapping states for the increased lifetime of the $\text{PCN}^{\bullet-}$ species (Figure 16a). If $\text{K}_2\text{S}_2\text{O}_8$ is too scarce, not enough holes are transferred to PCN to be recombined with stored electrons. On the other hand, if $\text{K}_2\text{S}_2\text{O}_8$ is too abundant all stored electrons are consumed quickly. Therefore, an optimal concentration of $\text{K}_2\text{S}_2\text{O}_8$ is needed for extended afterglow ECL. Increasing t_1 has the same effect as adding $\text{K}_2\text{S}_2\text{O}_8$: more $\text{SO}_4^{\bullet-}$ is generated in reaction (2) and stored electrons are quenched sooner. Nevertheless, a minimum charging time is needed to generate sufficient stored electrons. Hence, an ideal t_1 exists, too.

In ECL, the analyte is typically quantified by measuring the luminescence intensity. Instead, afterglow ECL introduces the use of the afterglow luminescence duration as a probing signal. For example, the lifetime of ECL is decreased in the presence of electron scavengers. Indeed, when H_2O_2 was introduced in concentrations ranging from 0.5 to 100 mM, the afterglow ECL decreased from 60 to 0.9 s. Taking the logarithm of the H_2O_2 , a linear calibration curve was made (Figure 16b). The ideal analyte should scavenge electrons from the semiconductor efficiently enough but should not be reduced directly at the electrode for thermodynamic or kinetic reasons. However, a careful experimental design lifts this requirement. For example, assuming that an analyte was so oxidative that it would be reduced at the electrode, the afterglow mechanism circumvents this problem if the species to quantify is added immediately after removing the bias. The parasitic electrochemical reaction would be avoided but the electron scavenging would still reduce the afterglow ECL duration.

In summary, analytical methods based on electron-storing semiconductors have quite opposite requirements compared with other applications. While in most cases a slow discharge process is beneficial (e.g., for time-delayed catalysis or memory storage), sensors need a very efficient and fast discharging time, which is a low R_{DC} value. At the same time, they require a very

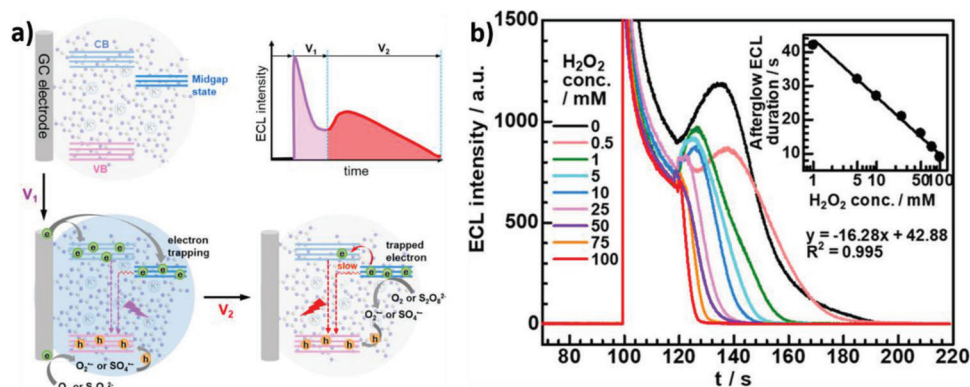


Figure 16. a) Scheme of the proposed mechanism of afterglow ECL from a $\text{CN}_x\text{NS-1.6}$ electrode in a $\text{K}_2\text{S}_2\text{O}_8$ solution. b) Calibration of $\text{CN}_x\text{NS-1.6}$ afterglow ECL duration versus H_2O_2 concentration (V_1 : 1.0 V vs Ag/AgCl, t_1 : 10 s, 1 mM $\text{K}_2\text{S}_2\text{O}_8$). Reproduced with permission.^[148] Copyright 2023. American Chemical Society.

high R_{PC} , so that many analytical cycles can be repeated every few minutes or seconds.

7. Microswimmers

In 2020, a very innovative application of photocharged semiconductors was proposed. Sridhar and co-workers demonstrated that nanoparticles based on PHIs were propelled in solution by light, preserving high mobility for several minutes even after the irradiation was switched off.^[152] This technology pertains to microswimmers, that is micro or nano-sized robots capable of moving into a liquid medium upon certain stimuli.^[153] Self-propelling colloidal motors are largely relevant to biomedicine, especially for drug delivery.^[154] Propelling agents can be sacrificial chemical agents as well as magnetic, electric, or acoustic fields.^[155] Chemical agents—usually from gas-generating reactions catalyzed by the microswimmers themselves—represent the most common propulsion strategy.^[156] The major drawback of such a system is the need for a continuous supply of fuel. Instead, light is an inexpensive stimulus to induce motion in photocatalytic materials with no generation of chemical waste.^[157,158] Light-driven motion at the nanoscale is usually realized with Janus particles, that is particles made of two chemically different halves.^[159] Motion can be either generated by self-electrophoresis or diffusiophoresis.^[160] In self-electrophoresis, a cathodic and an anodic reactions take place on opposite sides of the particle, generating a gradient of ionic species. The electrically charged Janus particle moves in the self-generated electric field by electrophoresis (Figure 17a). In diffusiophoresis, a chemical species, either ionic or neutral, is mostly produced on one side of the particle and the motion is induced by diffusion along concentration gradients. Figure 17b illustrates diffusiophoresis when the electrolyte is the species forming a concentration gradient.

In the work by Sridhar and co-workers, PHI spherical Janus particles capped with a catalytic Pd, Au, or SiO_2 layer were investigated as light-propelled microswimmers with charge-storing properties.^[152] The authors first observed that all these particles were capable of phototaxis even in the absence of a sacrificial electron donor, reaching an average speed of $10 \mu\text{m s}^{-1}$ in water when illuminated with a Xe lamp. This was already comparable with state-of-the-art TiO_2 microswimmers that are only powered

by UV light. The speed doubled in the presence of methanol as a hole scavenger. Then, H_2O_2 was investigated as a fuel, where its disproportionation serves as propelling reaction. Au-capped particles moved faster than Pt-capped, while the speed was much lower for non-catalytic SiO_2 . Cyclic voltammetry measurements showed that Pt was much more redox active than Au. Thus, it was assumed that H_2O_2 decomposition occurred with similar rates on both sides of Pt-capped particles, leading to a lower speed than Au-PHI. Nevertheless, the strong light response of Pt motivated the authors to use Pt-PHI particles for prolonged phototaxis in the dark. The hypothesis was that electrons photogenerated on the Pt side could quench holes at the interface with PHI, promoting charge storage (Figure 18a). The same strategy was indeed previously demonstrated for Au–Pt particles.^[161] Particles shifted from Brownian to ballistic motion during 7 s of illumination, and the same speed was maintained in the following 7 s after switching off the light (Figure 18b). In their best attempt, after 30 s of photocharging the particles retained ballistic motion

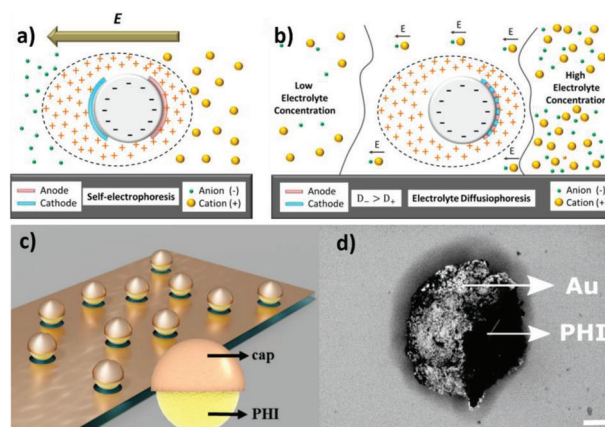


Figure 17. Schemes of a) self-electrophoresis and b) diffusiophoresis generating propulsion in Janus particles microswimmers. Reproduced with permission.^[158] Copyright 2018. American Chemical Society. c) Janus microswimmer particles prepared by sputtering Pt, Au, or SiO_2 on PHI nanospheres. d) SEM image of an Au-capped PHI Janus particle illustrated in c) (scale bar: 400 nm). Reproduced with permission.^[152] Copyright 2020. National Academy of Sciences.

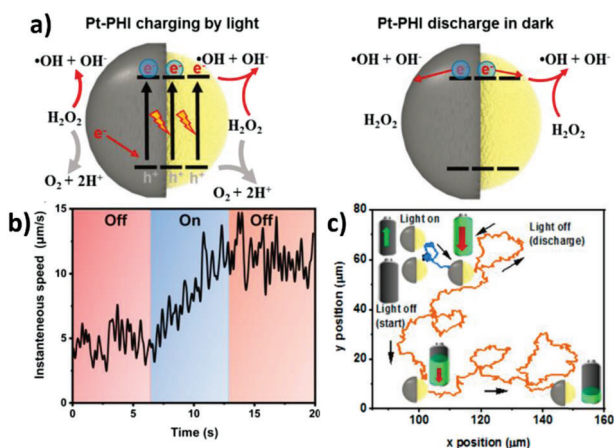


Figure 18. a) Scheme of the proposed charge and discharge mechanism in Pt-capped PHI particles with time-delayed ballistic motion. b) Evolution of speed of Pt-capped PHI particles under consecutive 7 s dark-light-dark cycles in a 1% H_2O_2 solution. c) Trajectory of Pt-capped PHI particles in the dark (10 s, black trace), under illumination (5 s, blue trace), and after switching off light (105 s, orange trace). Reproduced with permission.^[152] Copyright 2020. National Academy of Sciences.

for up to 30 min. The observed behavior was compared to that of a “solar battery”, where a nanorobot can be charged with light to cover long trajectories in the dark before it is fully discharged (Figure 18c).

PHIs and other layered organic polymers like covalent organic frameworks have recently stimulated great interest to develop light-driven microswimmers, because of their high interlayer ion-storing capacity.^[162] To date, the work by Sridhar et al. is the only report of a photochargeable nanomotor. As for many other applications of photochargeable semiconductors, the charge/discharge time ratio is a key figure of merit. In the context of photocharged microswimmers application for drug delivery, ideally they should be activated with light prior to administration to a patient and allowed to travel to the target center in the body with no further stimuli. The outcomes hold promise for the application of bio-compatible polymeric carbon nitrides for time-delayed drug delivery and, more generally, for autonomous systems powered by metal-free solar batteries. The design of PHI-based solar batteries is already emerging.^[16,28]

8. Conclusions and Perspectives

Data previously collected from 52 publications and updated with more than 90 new entries were analyzed to determine key parameters that affect the performance of light-induced charge-storing in semiconductors, as well as possible correlations between them. Some trends were identified, that could possibly guide the design of semiconducting materials for applications based on photocharging: i) bigger particles store more electrons; ii) for TiO_2 nanoparticles, the higher the storing capacity, the faster the photocharging; iii) bigger particles discharge more slowly; iv) semiconductors discharge faster with more concentrated electron scavengers. More importantly, by reviewing this broad category of materials we found a range of potential applications that have been largely neglected, overshadowed by “dark

photocatalysis”. Below, we summarize the most desirable features that a photochargeable semiconductor should have for each of them and we recommend suitable materials in Table 3.

Charge storage is at the foundation of state-of-the-art memory-storing devices, which mostly rely on electric rather than optical switching. Light-induced accumulation will probably be more scalable for transition-based memories with floating gates. Information can be written via optical pulses (charging) and erased electrically (discharging). Memory devices must have a low discharging rate for low volatility. Thus, appropriate designs should be made to prevent atmospheric oxygen from scavenging accumulated electrons. This is usually not an issue because floating gates come with protective layers. The writing process should take a few seconds or minutes, which means high photocharging rates are desirable. Materials with higher capacity generate higher ON/OFF current ratios, but this is generally not necessary because the two states only need to be qualitatively distinct (1 or 0). Quantum dots including CdSe, ZnS, and perovskites already proved suitable, given their slow discharging rate. Indeed, particles with diameters ranging from 3 to 15 nm were used,^[56,58,61,63] which is in the upper range of sizes reported for semiconductor photocharging, giving the lowest R_{DC} . It should be reminded that the size of QDs also influences their absorbing properties, with smaller particles absorbing shorter wavelengths. TiO_2 nanoparticles bigger than 15 nm also have appropriate low R_{DC} , although their optical properties are limited to UV. Such limitation might be overcome through heterojunction with low bandgap semiconductors like WO_3 , possibly in core-shell morphologies. Furthermore, polymeric carbon nitrides in optoelectronics TBM devices have not been reported yet.

The slow release of photoaccumulated charge is extremely relevant to electrodes and coatings for prolonged cathodic protection to prevent corrosion of metals and steel. In the naval sector, a semiconductor-based photoelectrode placed on the hull should accumulate electrons under daylight and slowly release them during the night to the steel counter electrode. The more electrons are accumulated, the lower the open circuit voltage of steel, and the more extended the post-irradiation protection. Conversely, the rate of photocharging is not important, because materials are supposed to be under irradiation for hours during the daytime. Bigger particle volumes are expected to favor both charge-storing capacity and slow discharging times. Moreover, particles should be non-porous to prevent fast leakage of counter-ions from the semiconductor to the solution. Indeed, R_{DC} was higher in highly porous metal-organic frameworks.^[25,26] So far, researchers considered a variety of bulk TiO_2 heterojunctions with visible light-absorbing semiconductors. WO_3 and SnO_2 were the preferred ones because they can store electrons in W(V) and Sn(III) bronzes, respectively.^[13,94] Nevertheless, materials with intrinsic photocharging should be given more attention. PCN is a promising alternative given its negative (≈ -0.1 V vs Ag/AgCl) CB edge, although stability and adhesion on electrodes should be improved, and coupling with more oxidative semiconductors or catalysts for water oxidation is essential. The addition of graphene layers might also help electron trapping in the aromatic structure. Unfortunately, most photoanodes for anti-corrosion still need Na_2S as a sacrificial hole scavenger. Therefore, the incorporation of oxygen-evolving catalysts will be necessary for real-world applications.

Table 3. Recommended features and materials for each of the applications of photocharged semiconductors discussed in this review.

Application	Desirable features		Recommended materials
	Capacity [δ_{\max}]	Rate of photocharging R_{PC}	
Dark photocatalysis Memory devices	High	Not relevant	CdSe, CdS, ZnS, and other QDs Large (> 15 nm) TiO ₂ NPs TiO ₂ /WO ₃ heterojunctions Core-shell geometries
	Not relevant	High	
Photocathodic protection	High	Not relevant	Large, non-porous particles PCN with enhanced stability Adsorbed on graphene coupled with OER catalyst
Sensors	Tunable	Very high	Metal-organic frameworks Poly (heptazine imides)
Microswimmers	High	High	Highly porous anatase or other semiconductors High concentration of hole scavenger
		Low	High concentration and diffusivity of propeller (electron scavenger) Polymeric carbon nitrides Non-porous semiconductors

Photocharged semiconductors can be used to quantify suitable electron or hole scavengers. The concentration of the analyte determines the extent of discharge or charge of the semiconductors, respectively. In the first case, the analyte depletes electrons from a previously photocharged semiconductor. In the second case, the analyte enhances the amount of charge stored during irradiation working as a hole scavenger. The residual or increased number of stored electrons can be found via different methods, whether colorimetric or electrochemical. Contrary to most other applications, analytical devices require fast discharge rates. For a quick response, electrons should be discharged as fast as possible. At the same time, the semiconductors should be charged for every single measurement, that is many times in a short period of time. Thus, a very high rate of photocharging is also needed. The number of stored electrons determines the analytical range, although the sensitivity only depends on how the variation in stored charges affects measurable properties (e.g., photochromism). Because of their high porosity, fast discharging, and high capacity, metal-organic frameworks are good candidates. In crystalline polymeric carbon nitrides like PHIs, the charge-storing capacity can be tuned varying the composition of the precursor materials.^[144] There are currently no reliable strategies to adjust R_{PC} , although it was shown to increase for TiO₂ particles with increasing capacity. Again, mesoporous materials might facilitate counter-ions intercalation and release.

Finally, photocharged microswimmers based on polymeric carbon nitrides have been reported only recently. Here, the transition from the diffusive to the ballistic motion regime of a nanoparticle is induced by a photocatalyzed chemical reaction. For this reason, this application can be considered a subfield of dark photocatalysis. Microrobots for drug delivery could be charged in vitro and retain high mobility in the dark after injection into the body. To ensure directionality, asymmetric Janus particles with propelling and inert faces are usually chosen. For durable propulsion, particles should store many electrons with a slow and steady discharge. Preferentially, particles should be charged quickly to receive multiple “pushes” while swimming. Here, the concentration of hole scavengers plays a major role. Particles should be first charged in an excess of electron donor and then transferred into the desired environment or diluted. On the other hand, the chemical that generates propulsion in the catalytic reaction should have a higher local concentration on the particles, that is higher diffusivity. It is not easy to recommend an ideal semiconductor for microswimmers, since additional parameters (e.g., cytotoxicity) should be considered. Polymeric carbon nitrides seem a viable choice because of their high biocompatibility, while non-porous anatase might also be considered.

In this work, we showcased potential research directions on photochargeable semiconductors beyond dark photocatalysis. We also hope that the list of materials found in the updated database will inspire experts from different fields to investigate new designs.

Supporting Information

Supporting Information is available from the Wiley Online Library or from the author.

Acknowledgements

O.S. acknowledges Prof. Markus Antonietti and the Max Planck Society for supporting this work.

Open access funding enabled and organized by Projekt DEAL.

Conflict of Interest

The authors declare no conflict of interest.

Keywords

anti-corrosion, dark photocatalysis, memory storage, microswimmers, photocharging, semiconductors, sensors

Received: May 6, 2023

Revised: July 18, 2023

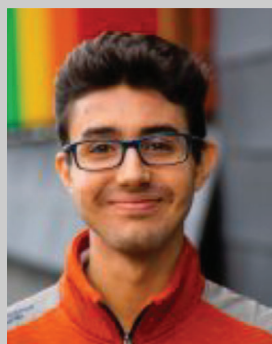
Published online: August 3, 2023

- [1] a) M. Grätzel, *Inorg. Chem.* **2005**, *44*, 6841; b) P. K. Nayak, S. Mahesh, H. J. Snaith, D. Cahen, *Nat. Rev. Mater.* **2019**, *4*, 269.
- [2] a) C. Klingshirn, H. Haug, *Phys. Rep.* **1981**, *70*, 315; b) B. Liu, H. Wu, I. P. Parkin, *ACS Omega* **2020**, *5*, 14847.
- [3] a) A. Savateev, I. Ghosh, B. König, M. Antonietti, *Angew. Chem., Int. Ed.* **2018**, *57*, 15936; b) H. Kisch, *Angew. Chem., Int. Ed.* **2013**, *52*, 812; c) A. Fu, W. Gu, C. Larabell, A. P. Alivisatos, *Curr. Opin. Neurobiol.* **2005**, *15*, 568; d) C. Stefania, B. Alberto, *Adv. Photonics* **2021**, *3*, 054001; e) Y. Xing, Z. Xia, J. Rao, *IEEE Trans. Nanobiosci.* **2009**, *8*, 4; f) M. C. D. Santos, W. R. Algar, I. L. Medintz, N. Hildebrandt, *TrAC, Trends Anal. Chem.* **2020**, *125*, 115819.
- [4] a) I. Bedja, S. Hotchandani, P. V. Kamat, *J. Phys. Chem.* **1993**, *97*, 11064; b) X. X. Zou, G.-D. Li, K. X. Wang, L. Li, J. Su, J.-S. Chen, *Chem. Commun.* **2010**, *46*, 2112.
- [5] O. Savateev, *Adv. Energy Mater.* **2022**, *12*, 2200352.
- [6] a) A. Henglein, *Ber. Bunsenges. Phys. Chem.* **1982**, *86*, 241; b) R. F. Howe, M. Grätzel, *J. Phys. Chem.* **1985**, *89*, 4495.
- [7] H. H. Mohamed, C. B. Mendive, R. Dillert, D. W. Bahnemann, *J. Phys. Chem. A* **2011**, *115*, 2139.
- [8] a) H. H. Mohamed, R. Dillert, D. W. Bahnemann, *J. Phys. Chem. C* **2011**, *115*, 12163; b) D. Zywitzki, H. Jing, H. Tüysüz, C. K. Chan, *J. Mater. Chem. A* **2017**, *5*, 10957; c) H. H. Mohamed, R. Dillert, D. W. Bahnemann, *J. Photochem. Photobiol. A Chem.* **2011**, *217*, 271.
- [9] Y. Ke, J. Chen, G. Lin, S. Wang, Y. Zhou, J. Yin, P. S. Lee, Y. Long, *Adv. Energy Mater.* **2019**, *9*, 1902066.
- [10] M. Takeuchi, G. Martra, S. Coluccia, M. Anpo, *J. Phys. Chem. C* **2007**, *111*, 9811.
- [11] C. T. Saouma, S. Richard, S. Smolders, M. F. Delley, R. Ameloot, F. Vermoortele, D. E. De Vos, J. M. Mayer, *J. Am. Chem. Soc.* **2018**, *140*, 16184.
- [12] A. Rogolino, I. F. Silva, N. V. Tarakina, M. A. R. da Silva, G. F. S. R. Rocha, M. Antonietti, I. F. Teixeira, *ACS Appl. Mater. Interfaces* **2022**, *14*, 49820.
- [13] Y. Takahashi, T. Tatsuma, *Electrochem. Commun.* **2008**, *10*, 1404.
- [14] E. Y. Tsui, K. H. Hartstein, D. R. Gamelin, *J. Am. Chem. Soc.* **2016**, *138*, 11105.
- [15] M. Ghini, N. Curreli, A. Camellini, M. Wang, A. Asaithambi, I. Kriegel, *Nanoscale* **2021**, *13*, 8773.
- [16] A. Gouder, F. Podjaski, A. Jiménez-Solano, J. Kröger, Y. Wang, B. V. Lotsch, *Energy Environ. Sci.* **2023**, *16*, 1520.
- [17] V. W. Lau, D. Klose, H. Kasap, F. Podjaski, M.-C. Pignié, E. Reisner, G. Jeschke, B. V. Lotsch, *Angew. Chem., Int. Ed.* **2017**, *56*, 510.
- [18] a) Y. Markushyna, P. Lamagni, C. Teutloff, J. Catalano, N. Lock, G. Zhang, M. Antonietti, A. Savateev, *J. Mater. Chem. A* **2019**, *7*, 24771; b) S. Mazzanti, C. Schritt, K. ten Brummelhuis, M. Antonietti, A. Savateev, *Exploration* **2021**, *1*, 20210063; c) J. Kröger, F. Podjaski, G. Savasci, I. Moudrakovski, A. Jiménez-Solano, M. W. Terban, S. Bette, V. Duppel, M. Joos, A. Senocrate, R. Dinnebier, C. Ochsenfeld, B. V. Lotsch, *Adv. Mater.* **2022**, *34*, 2107061; d) S. Mazzanti, Y. Markushyna, O. Savateev, *ChemCatChem* **2023**, *15*, 202201388.
- [19] H. Schlomberg, J. Kröger, G. Savasci, M. W. Terban, S. Bette, I. Moudrakovski, V. Duppel, F. Podjaski, R. Siegel, J. Senker, R. E. Dinnebier, C. Ochsenfeld, B. V. Lotsch, *Chem. Mater.* **2019**, *31*, 7478.
- [20] J. N. Schrauben, R. Hayoun, C. N. Valdez, M. Braten, L. Fridley, J. M. Mayer, *Science* **2012**, *336*, 1298.
- [21] W. K. Liu, K. M. Whitaker, A. L. Smith, K. R. Kittilstved, B. H. Robinson, D. R. Gamelin, *Phys. Rev. Lett.* **2007**, *98*, 186804.
- [22] F. Podjaski, J. Kröger, B. V. Lotsch, *Adv. Mater.* **2018**, *30*, 1705477.
- [23] M. Favaro, B. Jeong, P. N. Ross, J. Yano, Z. Hussain, Z. Liu, E. J. Crumlin, *Nat. Commun.* **2016**, *7*, 12695.
- [24] a) Q. Ruan, X. Xi, B. Yan, L. Kong, C. Jiang, J. Tang, Z. Sun, *Chem* **2023**, *9*, 1850; b) M. P. Ravikumar, S. Bharathkumar, B. Urupalli, M. K. Murikinati, S. Muthukonda Venkatakrishnan, S. Mohan, *Energy Fuels* **2022**, *36*, 11503; c) J. Fang, T. Debnath, S. Bhattacharyya, M. Döblinger, J. Feldmann, J. K. Stolarczyk, *Nat. Commun.* **2020**, *11*, 5179.
- [25] Y. Pan, J. Wang, S. Chen, W. Yang, C. Ding, A. Waseem, H.-L. Jiang, *Chem. Sci.* **2022**, *13*, 6696.
- [26] P. M. Stanley, F. Sixt, J. Warnan, *Adv. Mater.* **2023**, *35*, 2207280.
- [27] a) L. Zhang, Y. Wang, *Angew. Chem., Int. Ed.* **2023**, *62*, e202219076; b) O. Samuel, M. H. D. Othman, R. Kamaludin, O. Sinsamphanh, H. Abdullah, M. H. Puteh, T. A. Kurniawan, *Ceram. Int.* **2022**, *48*, 5845; c) J. W.-h. Lau, B. V. Lotsch, *Adv. Energy Mater.* **2022**, *12*, 2101078.
- [28] F. Podjaski, B. V. Lotsch, *Adv. Energy Mater.* **2021**, *11*, 2003049.
- [29] M. J. Turo, L. Chen, C. E. Moore, A. M. Schimpf, *J. Am. Chem. Soc.* **2019**, *141*, 4553.
- [30] M. Dan-Hardi, C. Serre, T. Frot, L. Rozes, G. Maurin, C. Sanchez, G. Férey, *J. Am. Chem. Soc.* **2009**, *131*, 10857.
- [31] B. Bueken, F. Vermoortele, D. E. P. Vanpoucke, H. Reinsch, C.-C. Tsou, P. Valvekens, T. De Baerdemaeker, R. Ameloot, C. E. A. Kirschhock, V. Van Speybroeck, J. M. Mayer, D. De Vos, *Angew. Chem., Int. Ed.* **2015**, *54*, 13912.
- [32] a) G. Sahara, O. Ishitani, *Inorg. Chem.* **2015**, *54*, 5096; b) Z. Fu, X. Wang, A. M. Gardner, X. Wang, S. Y. Chong, G. Neri, A. J. Cowan, L. Liu, X. Li, A. Vogel, R. Clowes, M. Bilton, L. Chen, R. S. Sprick, A. I. Cooper, *Chem. Sci.* **2020**, *11*, 543; c) H.-P. Liang, A. Acharyya, D. A. Anito, S. Vogl, T.-X. Wang, A. Thomas, B. H. Han, *ACS Catal.* **2019**, *9*, 3959; d) P. M. Stanley, J. Warnan, *Energies* **2021**, *14*, 4260.
- [33] a) A. M., J. M., M. Ashokkumar, P. Arunachalam, *Appl. Catal., A* **2018**, *555*, 47; b) Y. Park, K. J. McDonald, K. S. Choi, *Chem. Soc. Rev.* **2013**, *42*, 2321; c) F. F. Abdi, L. Han, A. H. M. Smets, M. Zeman, B. Dam, R. van de Krol, *Nat. Commun.* **2013**, *4*, 2195.
- [34] a) R. a. He, S. Cao, P. Zhou, J. Yu, *Chin. J. Catal.* **2014**, *35*, 989; b) N. S. Azhar, M. F. M. Taib, O. H. Hassan, M. Z. A. Yahya, A. M. M. Ali, *Mater. Res. Express* **2017**, *4*, 034002; c) Z. Zhao, H. Dai, J. Deng, Y. Liu, C. T. Au, *Solid State Sci.* **2013**, *18*, 98; d) H. Arshad, M. U. Tahir, F. Rehman, L. Wang, J. Wang, X. Su, C. Yang, *Appl. Surf. Sci.* **2022**, *574*, 151678.
- [35] H. Son, Y. Kim, *J. Phys. Chem. Solids* **2022**, *167*, 110781.
- [36] M. Wang, G. Tan, B. Zhang, Y. Wang, Y. Bi, Q. Yang, Y. Liu, T. Liu, Z. Wang, H. Ren, L. Lv, A. Xia, L. Yin, Q. Yuan, W. Liu, Y. Liu, *Appl. Catal., B* **2023**, *321*, 122052.
- [37] J. Wang, P. Li, Y. Wang, Z. Liu, D. Wang, J. Liang, Q. Fan, *Adv. Sci.* **2023**, *10*, 2205542.
- [38] J. Kröger, A. Jiménez-Solano, G. Savasci, P. Rovó, I. Moudrakovski, K. Küster, H. Schlomberg, H. A. Vignolo-González, V. Duppel, L.

- Grunenberg, C. B. Dayan, M. Sitti, F. Podjaski, C. Ochsenfeld, B. V. Lotsch, *Adv. Energy Mater.* **2021**, *11*, 2003016.
- [39] C. Adler, S. Selim, I. Kivrtsov, C. Li, D. Mitoraj, B. Dietzek, J. R. Durrant, R. Beranek, *Adv. Funct. Mater.* **2021**, *31*, 2105369.
- [40] Z. Chen, A. Savateev, S. Pronkin, V. Papaefthimiou, C. Wolff, M. G. Willinger, E. Willinger, D. Neher, M. Antonietti, D. Dontsova, *Adv. Mater.* **2017**, *29*, 1700555.
- [41] a) A. Savateev, N. V. Tarakina, V. Strauss, T. Hussain, K. ten Brummelhuis, J. M. Sánchez Vadillo, Y. Markushyna, S. Mazzanti, A. P. Tyutyunnik, R. Walczak, M. Oschatz, D. M. Galdi, A. Karton, M. Antonietti, *Angew. Chem., Int. Ed.* **2020**, *59*, 15061; b) A. Savateev, S. Pronkin, J. D. Epping, M. G. Willinger, C. Wolff, D. Neher, M. Antonietti, D. Dontsova, *ChemCatChem* **2017**, *9*, 167.
- [42] G. Seo, Y. Saito, M. Nakamichi, K. Nakano, K. Tajima, K. Kanai, *Sci. Rep.* **2021**, *11*, 17833.
- [43] N. Karjule, R. Phatake, M. Volokh, I. Hod, M. Shalom, *Small Methods* **2019**, *3*, 1900401.
- [44] S. Amthor, S. Knoll, M. Heiland, L. Zedler, C. Li, D. Nauroozi, W. Tobiaschus, A. K. Mengele, M. Anjass, U. S. Schubert, B. Dietzek-Ivanšić, S. Rau, C. Streb, *Nat. Chem.* **2022**, *14*, 321.
- [45] a) A. Liu, L. Gedda, M. Axelsson, M. Pavliuk, K. Edwards, L. Hammarström, H. Tian, *J. Am. Chem. Soc.* **2021**, *143*, 2875; b) A. Sekar, J. M. Moreno-Naranjo, Y. Liu, J.-H. Yum, B. P. Darwich, H.-H. Cho, N. Guijarro, L. Yao, K. Sivula, *ACS Appl. Mater. Interfaces* **2022**, *14*, 8191; c) L. Wang, R. Fernández-Terán, L. Zhang, D. L. A. Fernandes, L. Tian, H. Chen, H. Tian, *Angew. Chem., Int. Ed.* **2016**, *55*, 12306; d) H.-H. Cho, L. Yao, J.-H. Yum, Y. Liu, F. Boudoire, R. A. Wells, N. Guijarro, A. Sekar, K. Sivula, *Nat. Catal.* **2021**, *4*, 431; e) Y. Wang, A. Vogel, M. Sachs, R. S. Sprick, L. Wilbraham, S. J. A. Moniz, R. Godin, M. A. Zwijnenburg, J. R. Durrant, A. I. Cooper, J. Tang, *Nat. Energy* **2019**, *4*, 746.
- [46] a) J. Kosco, M. Bidwell, H. Cha, T. Martin, C. T. Howells, M. Sachs, D. H. Anjum, S. G. Lopez, L. Zou, A. Wadsworth, W. Zhang, L. Zhang, J. Tellam, R. Sougrat, F. Laquai, D. M. DeLongchamp, J. R. Durrant, I. McCulloch, *Nat. Mater.* **2020**, *19*, 559; b) Y. Bai, L. Wilbraham, B. J. Slater, M. A. Zwijnenburg, R. S. Sprick, A. I. Cooper, *J. Am. Chem. Soc.* **2019**, *141*, 9063.
- [47] J. Kosco, S. Gonzalez-Carrero, C. T. Howells, T. Fei, Y. Dong, R. Sougrat, G. T. Harrison, Y. Firdaus, R. Sheelamanthula, B. Purushothaman, F. Moruzzi, W. Xu, L. Zhao, A. Basu, S. De Wolf, T. D. Anthopoulos, J. R. Durrant, I. McCulloch, *Nat. Energy* **2022**, *7*, 340.
- [48] a) H. Kasap, C. A. Caputo, B. C. M. Martindale, R. Godin, V. W.-h. Lau, B. V. Lotsch, J. R. Durrant, E. Reisner, *J. Am. Chem. Soc.* **2016**, *138*, 9183; b) W. Yang, R. Godin, H. Kasap, B. Moss, Y. Dong, S. A. J. Hillman, L. Steier, E. Reisner, J. R. Durrant, *J. Am. Chem. Soc.* **2019**, *141*, 11219; c) M. Sachs, H. Cha, J. Kosco, C. M. Aitchison, L. Francàs, S. Corby, C. L. Chiang, A. A. Wilson, R. Godin, A. Fahey-Williams, A. I. Cooper, R. S. Sprick, I. McCulloch, J. R. Durrant, *J. Am. Chem. Soc.* **2020**, *142*, 14574.
- [49] A. Fazio, *MRS Online Proc. Libr.* **2004**, *830*, 31.
- [50] J. S. Lee, *Electron. Mater. Lett.* **2011**, *7*, 175.
- [51] Z. Lv, Y. Wang, J. Chen, J. Wang, Y. Zhou, S.-T. Han, *Chem. Rev.* **2020**, *120*, 3941.
- [52] a) M. E. Gemayel, K. Börjesson, M. Herder, D. T. Duong, J. A. Hutchison, C. Ruzié, G. Schweicher, A. Salleo, Y. Geerts, S. Hecht, E. Orgiu, P. Samorì, *Nat. Commun.* **2015**, *6*, 6330; b) J. Zhuang, W. S. Lo, L. Zhou, Q. J. Sun, C. F. Chan, Y. Zhou, S. T. Han, Y. Yan, W. T. Wong, K. L. Wong, V. A. L. Roy, *Sci. Rep.* **2015**, *5*, 14998.
- [53] a) X. Gao, C.-H. Liu, X. J. She, Q. L. Li, J. Liu, S. D. Wang, *Org. Electron.* **2014**, *15*, 2486; b) S. Dutta, K. S. Narayan, *Adv. Mater.* **2004**, *16*, 2151.
- [54] X. Wu, S. Lan, D. Hu, Q. Chen, E. Li, Y. Yan, H. Chen, T. Guo, *J. Mater. Chem. C* **2019**, *7*, 9229.
- [55] Y. Wang, Z. Lv, J. Chen, Z. Wang, Y. Zhou, L. Zhou, X. Chen, S. T. Han, *Adv. Mater.* **2018**, *30*, 1802883.
- [56] C.-C. Chen, M.-Y. Chiu, J.-T. Sheu, K.-H. Wei, *Appl. Phys. Lett.* **2008**, *92*, 143105.
- [57] W. U. Huynh, J. J. Dittmer, A. P. Alivisatos, *Science* **2002**, *295*, 2425.
- [58] S.-T. Han, Y. Zhou, L. Zhou, Y. Yan, L. B. Huang, W. Wu, V. A. L. Roy, *J. Mater. Chem. C* **2015**, *3*, 3173.
- [59] H. Hu, G. Wen, J. Wen, L.-B. Huang, M. Zhao, H. Wu, Z. Sun, *Adv. Sci.* **2021**, *8*, 2100513.
- [60] Q. Li, T. Li, Y. Zhang, Y. Yu, Z. Chen, L. Jin, Y. Li, Y. Yang, H. Zhao, J. Li, J. Yao, *Org. Electron.* **2020**, *77*, 105461.
- [61] J. Wen, H. Hu, G. Wen, S. Wang, Z. Sun, S. Ye, *J. Phys. D: Appl. Phys.* **2021**, *54*, 114002.
- [62] a) Y. Kim, S. Cho, H. Kim, S. Seo, H. U. Lee, J. Lee, H. Ko, M. Chang, B. Park, *J. Phys. D: Appl. Phys.* **2017**, *50*, 365303; b) R. Liu, C. Hou, X. Liang, Z. Wu, G. Tai, *Nano Res.* **2022**, *97*, 107189.
- [63] Y. J. Jeong, D. J. Yun, S. H. Noh, C. E. Park, J. Jang, *ACS Nano* **2018**, *12*, 7701.
- [64] S. Carrara, *IEEE Sens. J.* **2021**, *21*, 12370.
- [65] J. J. Yang, D. B. Strukov, D. R. Stewart, *Nat. Nanotechnol.* **2013**, *8*, 13.
- [66] L. Chua, *IEEE Trans. Circuit Theory* **1971**, *18*, 507.
- [67] D. B. Strukov, G. S. Snider, D. R. Stewart, R. S. Williams, *Nature* **2008**, *453*, 80.
- [68] T. Shi, R. Wang, Z. Wu, Y. Sun, J. An, Q. Liu, *Small Struct.* **2021**, *2*, 2000109.
- [69] Y. Li, S. Long, Q. Liu, H. Lv, M. Liu, *Small* **2017**, *13*, 1604306.
- [70] H. S. P. Wong, H. Y. Lee, S. Yu, Y. S. Chen, Y. Wu, P. S. Chen, B. Lee, F. T. Chen, M. J. Tsai, *Proc. IEEE Inst. Electr. Electron Eng.* **2012**, *100*, 1951.
- [71] V. Gupta, S. Kapur, S. Saurabh, A. Grover, *J. Inst. Electron. Telecommun. Eng. (New Delhi)* **2020**, *37*, 377.
- [72] Y. Ho, G. M. Huang, P. Li, presented at 2009 IEEE/ACM Int. Conf. on Computer-Aided Design—Digest of Technical Papers, IEEE, Piscataway, NJ, USA **2009**.
- [73] J.-Y. Mao, L. Zhou, X. Zhu, Y. Zhou, S.-T. Han, *Adv. Opt. Mater.* **2019**, *7*, 1900766.
- [74] H. Fang, W. Hu, *Adv. Sci.* **2017**, *4*, 1700323.
- [75] Y. Wang, Z. Lv, Q. Liao, H. Shan, J. Chen, Y. Zhou, L. Zhou, X. Chen, V. A. L. Roy, Z. Wang, Z. Xu, Y.-J. Zeng, S.-T. Han, *Adv. Mater.* **2018**, *30*, 1800327.
- [76] Z. Lv, Y. Wang, Z. Chen, L. Sun, J. Wang, M. Chen, Z. Xu, Q. Liao, L. Zhou, X. Chen, J. Li, K. Zhou, Y. Zhou, Y.-J. Zeng, S.-T. Han, V. A. L. Roy, *Adv. Sci.* **2018**, *5*, 1800714.
- [77] a) Y. Wu, Y. Wei, Y. Huang, F. Cao, D. Yu, X. Li, H. Zeng, *Nano Res.* **2017**, *10*, 1584; b) J. Lee, S. Pak, Y. W. Lee, Y. Cho, J. Hong, P. Giraud, H. S. Shin, S. M. Morris, J. I. Sohn, S. Cha, J. M. Kim, *Nat. Commun.* **2017**, *8*, 14734; c) Y. Zhai, X. Yang, F. Wang, Z. Li, G. Ding, Z. Qiu, Y. Wang, Y. Zhou, S.-T. Han, *Adv. Mater.* **2018**, *30*, 1803563; d) X. Zhu, J. Lee, W. D. Lu, *Adv. Mater.* **2017**, *29*, 1700527; e) M. Ungureanu, R. Zazpe, F. Golmar, P. Stoliar, R. Llopis, F. Casanova, L. E. Hueso, *Adv. Mater.* **2012**, *24*, 2496; f) Z. Liu, P. Cheng, Y. Li, R. Kang, Z. Zhang, Z. Zuo, J. Zhao, *ACS Appl. Mater. Interfaces* **2021**, *13*, 58885.
- [78] X. Fang, Y. Lu, X. Chen, H. Cheng, H. Qiu, Y. Zheng, J. Zhu, *ACS Appl. Nano Mater.* **2022**, *5*, 14722.
- [79] R. Pappu, B. Recht, J. Taylor, N. Gershenfeld, *Science* **2002**, *297*, 2026.
- [80] a) M. Amani, D. Hjeij, presented at SPE Kuwait Oil and Gas Show and Conf. SPE, Mishref, Kuwait, **2015**; b) L. Li, M. Chakik, R. Prakash, *Sensors* **2021**, *21*, 2908.
- [81] M. Laleh, A. E. Hughes, W. Xu, I. Gibson, M. Y. Tan, *Int. Mater. Rev.* **2021**, *66*, 563.
- [82] a) J. Sun, H. Tang, C. Wang, Z. Han, S. Li, *Steel Res. Int.* **2022**, *93*, 2100450; b) R. K. Gupta, N. Birbilis, *Corros. Sci.* **2015**, *92*, 1.

- [83] Y. Bu, J. P. Ao, *Green Energy Environ.* **2017**, *2*, 331.
- [84] a) D. Xu, Y. Liu, Y. Liu, F. Chen, C. Zhang, B. Liu, *Mater. Des.* **2021**, *197*, 109235; b) A. Byrne, N. Holmes, B. Norton, *Mag. Concr. Res.* **2016**, *68*, 664.
- [85] V. S. Saji, *J. Electrochem. Soc.* **2020**, *167*, 121505.
- [86] H. Park, K. Y. Kim, W. Choi, *J. Phys. Chem. B* **2002**, *106*, 4775.
- [87] J. Yuan, S. Tsujikawa, *J. Electrochem. Soc.* **1995**, *142*, 3444.
- [88] H. Park, K. Y. Kim, W. Choi, *Chem. Commun.* **2001**, 281.
- [89] a) C. Wang, W. Gao, N. Liu, Y. Xin, X. Liu, X. Wang, Y. Tian, X. Chen, B. Hou, *Corros. Sci.* **2020**, *176*, 108920; b) C. Feng, Z. Chen, J. Jing, M. Sun, G. Lu, J. Tian, J. Hou, *Corros. Sci.* **2020**, *166*, 108441; c) X. Li, X. Wang, X. Ning, J. Lei, J. Shao, W. Wang, Y. Huang, B. Hou, *Appl. Surf. Sci.* **2018**, *462*, 155; d) X. Jiang, M. Sun, Z. Chen, J. Jing, C. Feng, *Corros. Sci.* **2020**, *176*, 108901.
- [90] X. Chen, G. Zhou, X. Wang, H. Xu, C. Wang, Q. Yao, J. Chi, X. Fu, Y. Wang, X. Yin, Z. Zhang, *Chemosphere* **2023**, *323*, 138194.
- [91] T. Tatsuma, S. Saitoh, Y. Ohko, A. Fujishima, *Chem. Mater.* **2001**, *13*, 2838.
- [92] J. H. Park, J. S. Kim, J. M. Park, *Surf. Coat. Technol.* **2013**, *236*, 172.
- [93] H. Park, A. Bak, T. H. Jeon, S. Kim, W. Choi, *Appl. Catal., B* **2012**, *115–116*, 74.
- [94] T. Tatsuma, S. Takeda, S. Saitoh, Y. Ohko, A. Fujishima, *Electrochem. Commun.* **2003**, *5*, 793.
- [95] Z.-C. Guan, X. Wang, P. Jin, Y.-Y. Tang, H.-P. Wang, G. L. Song, R. G. Du, *Corros. Sci.* **2018**, *143*, 31.
- [96] M. J. Zhou, Z. O. Zeng, L. Zhong, *Corros. Sci.* **2009**, *51*, 1386.
- [97] S. Q. Yu, Y. H. Ling, R. G. Wang, J. Zhang, F. Qin, Z. J. Zhang, *Appl. Surf. Sci.* **2018**, *436*, 527.
- [98] Y. Liang, Z. C. Guan, H.-P. Wang, R. G. Du, *Electrochem. Commun.* **2017**, *77*, 120.
- [99] W. Sun, S. Cui, N. Wei, S. Chen, Y. Liu, D. Wang, *J. Alloys Compd.* **2018**, *749*, 741.
- [100] J. Jing, Z. Chen, Y. Bu, L. Xu, *J. Electrochem. Soc.* **2016**, *163*, C928.
- [101] W. Liu, T. Du, Q. Ru, S. Zuo, Y. Cai, C. Yao, *Mater. Res. Bull.* **2018**, *102*, 399.
- [102] Q. Liu, J. Hu, Y. Liang, Z. C. Guan, H. Zhang, H.-P. Wang, R. G. Du, *J. Electrochem. Soc.* **2016**, *163*, C539.
- [103] a) R. Subasri, T. Shinohara, *Electrochem. Solid-State Lett.* **2004**, *7*, B17; b) R. Subasri, T. Shinohara, *Electrochem. Commun.* **2003**, *5*, 897; c) R. Subasri, T. Shinohara, K. Mori, *Sci. Technol. Adv. Mater.* **2005**, *6*, 501; d) R. Subasri, T. Shinohara, K. Mori, *J. Electrochem. Soc.* **2005**, *152*, B105; e) J. Zhang, Z. Ur Rahman, Y. Zheng, C. Zhu, M. Tian, D. Wang, *Appl. Surf. Sci.* **2018**, *457*, 516.
- [104] H. Li, X. Wang, Y. Liu, B. Hou, *Corros. Sci.* **2014**, *82*, 145.
- [105] J. Hu, Q. Liu, H. Zhang, C. D. Chen, Y. Liang, R. G. Du, C. J. Lin, *J. Mater. Chem. A* **2015**, *3*, 22605.
- [106] W. Liu, K. Yin, F. He, Q. Ru, S. Zuo, C. Yao, *Mater. Res. Bull.* **2019**, *113*, 6.
- [107] M. J. Zhou, N. Zhang, L. Zhang, J. H. Yan, *Mater. Corros.* **2013**, *64*, 996.
- [108] S.-S. Ge, Q.-X. Zhang, X.-T. Wang, H. Li, L. Zhang, Q. Y. Wei, *Surf. Coat. Technol.* **2015**, *283*, 172.
- [109] M. Sun, Z. Chen, *J. Electrochem. Soc.* **2015**, *162*, C96.
- [110] H. Li, Y. Li, M. Wang, Z. Niu, X. Wang, B. Hou, *Nanotechnology* **2018**, *29*, 435706.
- [111] M. Sun, Z. Chen, J. Li, J. Hou, F. Xu, L. Xu, R. Zeng, *Electrochim. Acta* **2018**, *269*, 429.
- [112] C. Han, Q. Shao, J. Lei, Y. Zhu, S. Ge, *J. Alloys Compd.* **2017**, *703*, 530.
- [113] Y. Nan, X. Wang, X. Ning, J. Lei, S. Guo, Y. Huang, J. Duan, *Surf. Coat. Technol.* **2019**, *377*, 124935.
- [114] X. Wang, Z. C. Guan, P. Jin, Y.-Y. Tang, G.-L. Song, G. K. Liu, R. G. Du, *Corros. Sci.* **2019**, *157*, 247.
- [115] Z.-C. Guan, H.-P. Wang, X. Wang, J. Hu, R. G. Du, *Corros. Sci.* **2018**, *136*, 60.
- [116] W. Wang, X. Wang, N. Wang, X. Ning, H. Li, D. Lu, X. Liu, Q. Zhang, Y. Huang, *Nanoscale Res. Lett.* **2018**, *13*, 295.
- [117] Y. Yang, Y. F. Cheng, *Electrochim. Acta* **2017**, *253*, 134.
- [118] H. Li, X. Wang, Q. Wei, X. Liu, Z. Qian, B. Hou, *Nanotechnology* **2017**, *28*, 225701.
- [119] Y. F. Zhu, L. Xu, J. Hu, J. Zhang, R.-G. Du, C. J. Lin, *Electrochim. Acta* **2014**, *121*, 361.
- [120] J. Li, H. Yun, C. J. Lin, *ECS Trans.* **2008**, *3*, 1.
- [121] Y. Liu, C. Xu, Z. Feng, *Appl. Surf. Sci.* **2014**, *314*, 392.
- [122] J. Zhang, R.-G. Du, Z.-Q. Lin, Y.-F. Zhu, Y. Guo, H.-Q. Qi, L. Xu, C.-J. Lin, *Electrochim. Acta* **2012**, *83*, 59.
- [123] J. Zhang, J. Hu, Y.-F. Zhu, Q. Liu, H. Zhang, R.-G. Du, C.-J. Lin, *Corros. Sci.* **2015**, *99*, 118.
- [124] Z.-Q. Lin, Y.-K. Lai, R.-G. Hu, J. Li, R.-G. Du, C. J. Lin, *Electrochim. Acta* **2010**, *55*, 8717.
- [125] H. Li, X. Wang, L. Zhang, B. Hou, *Corros. Sci.* **2015**, *94*, 342.
- [126] H. Li, X. Wang, L. Zhang, B. Hou, *Nanotechnology* **2015**, *26*, 155704.
- [127] J. Zhu, H. Li, X. Cui, Z. Yang, B. Chen, Y. Li, P. Zhang, J. Li, *J. Alloys Compd.* **2022**, *926*, 166901.
- [128] W. Zhang, H. Guo, H. Sun, R. Zeng, *Appl. Surf. Sci.* **2017**, *410*, 547.
- [129] D. Ding, Q. Hou, Y. Su, Q. Li, L. Liu, J. Jing, B. Lin, Y. Chen, *J. Mater. Sci.: Mater. Electron.* **2019**, *30*, 12710.
- [130] Y. Bu, Z. Chen, J. Yu, W. Li, *Electrochim. Acta* **2013**, *88*, 294.
- [131] J. Jing, Z. Chen, C. Feng, M. Sun, J. Hou, *J. Alloys Compd.* **2021**, *851*, 156820.
- [132] W. Li, T. Shen, Y. Wang, F. Liu, W. Li, *ACS Appl. Electron. Mater.* **2020**, *2*, 2180.
- [133] a) J. Jing, M. Sun, Z. Chen, J. Li, F. Xu, L. Xu, *J. Electrochem. Soc.* **2017**, *164*, C822; b) Q. Zhang, J. Jing, Z. Chen, M. Sun, J. Li, Y. Li, L. Xu, *J. Mater. Sci.: Mater. Electron.* **2019**, *30*, 15267; c) Y. Ma, H. Wang, L. Sun, E. Liu, G. Fei, J. Fan, Y.-M. Kang, *Chem. Eng. J.* **2022**, *429*, 132520; d) W. Li, Y. Wang, X. Yang, F. Liu, W. Li, *ACS Appl. Nano Mater.* **2019**, *2*, 7559.
- [134] a) C. Feng, Z. Chen, J. Tian, J. Jing, L. Ma, J. Hou, *J. Mater. Sci. Technol.* **2021**, *90*, 183; b) Y. Yang, M. Sun, Z. Chen, H. Xu, X. Wang, J. Duan, B. Hou, *Chem. Eng. J.* **2023**, *458*, 141458.
- [135] Q.-P. Li, F.-Q. Liu, X.-L. Mu, H.-W. Wang, B. Wu, W. Li, *J. Alloys Compd.* **2021**, *870*, 159340.
- [136] Y.-F. Zhu, R.-G. Du, W. Chen, H.-Q. Qi, C.-J. Lin, *Electrochem. Commun.* **2010**, *12*, 1626.
- [137] J. Li, H. Yun, C.-J. Lin, *J. Electrochem. Soc.* **2007**, *154*, C631.
- [138] X. Xie, L. Liu, R. Chen, G. Liu, Y. Li, F. Wang, *J. Electrochem. Soc.* **2018**, *165*, H3154.
- [139] National Association of Corrosion Engineers, in *SP0169 Control of External Corrosion on Underground or Submerged Metallic Piping Systems*, National Association of Corrosion Engineers, Houston, TX, **2013**.
- [140] M. Baudys, Š. Paušová, P. Praus, V. Brezová, D. Dvoranová, Z. Barbieriková, J. Krýsa, *Materials* **2020**, *13*, 3038.
- [141] M. Volokh, M. Shalom, *Ann. N. Y. Acad. Sci.* **2023**, *1521*, 5.
- [142] A. Savateev, B. Kurpil, A. Mishchenko, G. Zhang, M. Antonietti, *Chem. Sci.* **2018**, *9*, 3584.
- [143] X. D. Wang, O. S. Wolfbeis, *Chem. Soc. Rev.* **2014**, *43*, 3666.
- [144] D. Han, H. Yang, Z. Zhou, K. Wu, J. Ma, Y. Fang, Q. Hong, G. Xi, S. Liu, Y. Shen, Y. Zhang, *ACS Sens.* **2022**, *7*, 2328.
- [145] T. Hirakawa, P. V. Kamat, *Langmuir* **2004**, *20*, 5645.
- [146] A. Gouder, A. Jiménez-Solano, N. M. Vargas-Barbosa, F. Podjaski, B. V. Lotsch, *Mater. Horiz.* **2022**, *9*, 1866.
- [147] C. Pulignani, C. A. Mesa, S. A. J. Hillman, T. Uekert, S. Giménez, J. R. Durrant, E. Reisner, *Angew. Chem., Int. Ed.* **2022**, *61*, e202211587.
- [148] L. Chen, X. Zhu, J. Wei, L. Tian, C. Hu, X. Xiang, S. F. Zhou, *Anal. Chem.* **2023**, *95*, 2917.

- [149] Y. Li, M. Gecevicius, J. Qiu, *Chem. Soc. Rev.* **2016**, 45 8, 2090.
 [150] C. Cheng, Y. Huang, X. Tian, B. Zheng, Y. Li, H. Yuan, D. Xiao, S. Xie, M. M. F. Choi, *Anal. Chem.* **2012**, 84, 4754.
 [151] V. W. H. Lau, I. Moudrakovski, T. Botari, S. Weinberger, M. B. Mesch, V. Duppel, J. Senker, V. Blum, B. V. Lotsch, *Nat. Commun.* **2016**, 7, 12165.
 [152] V. Sridhar, F. Podjaski, J. Kröger, A. Jiménez-Solano, B.-W. Park, B. V. Lotsch, M. Sitti, *Proc. Natl. Acad. Sci. USA* **2020**, 117, 24748.
 [153] M. Sitti, in *Mobile Microrobotics*, MIT Press, Cambridge, MA, USA, **2017**.
 [154] a) M. Luo, Y. Feng, T. Wang, J. Guan, *Adv. Funct. Mater.* **2018**, 28, 1706100; b) P. Erkoc, I. C. Yasa, H. Ceylan, O. Yasa, Y. Alapan, M. Sitti, *Adv. Ther.* **2019**, 2, 1800064.
 [155] Y. Alapan, O. Yasa, B. Yigit, I. C. Yasa, P. Erkoc, M. Sitti, *Annu. Rev. Control Robot. Auton. Syst.* **2019**, 2, 205.
 [156] S. Sánchez, L. Soler, J. Katuri, *Angew. Chem., Int. Ed.* **2015**, 54, 1414.
 [157] L. Xu, F. Mou, H. Gong, M. Luo, J. Guan, *Chem. Soc. Rev.* **2017**, 46, 6905.
 [158] J. Wang, Z. Xiong, J. Zheng, X. Zhan, J. Tang, *Acc. Chem. Res.* **2018**, 51, 1957.
 [159] A. Walther, A. H. E. Müller, *Soft Matter* **2008**, 4, 663.
 [160] W. E. Uspal, *J. Chem. Phys.* **2019**, 150, 114903.
 [161] M. Kuron, P. Kreissl, C. Holm, *Acc. Chem. Res.* **2018**, 51, 2998.
 [162] a) V. Sridhar, F. Podjaski, Y. Alapan, J. Kröger, L. Grunenberg, V. Kishore, B. V. Lotsch, M. Sitti, *Sci. Rob.* 7, eabm1421; b) V. Sridhar, E. Yildiz, A. Rodríguez-Camargo, X. Lyu, L. Yao, P. Wrede, A. Aghakhani, B. M. Akolpoglu, F. Podjaski, B. V. Lotsch, M. Sitti, *Adv. Mater.* **2023**, 35, 2301126.



Andrea Rogolino received his B.Sc. (2020) and M.Sc. (2022) in Chemistry at the University of Padova, Italy, where he was a fellow student at the Galilean School of Higher Education. In 2021, he was a visiting student at the Max Planck Institute of Colloids and Interfaces in Potsdam, Germany. He is currently a Ph.D. candidate in the Reisner Lab at the University of Cambridge. He nurtures a strong passion for every field of Chemistry since his participation in the International Chemistry Olympiads in 2016 and 2017. His actual research interests are photo(electro)chemical devices for solar fuel production.



Oleksandr Savateev since 2017 has been leading the group “Innovative Heterogeneous Photocatalysis” at the Max Planck Institute of Colloids and Interfaces, Potsdam, Germany. Among his current scientific interests are graphitic carbon nitride materials applied as heterogeneous photocatalysts in organic synthesis and a platform for solar energy storage via photocharging.